3.7 TURBULENCE WITHIN AND ABOVE REAL AND ARTIFICIAL URBAN CANOPIES

Matthew A. Nelson*, Michael J. Brown
Los Alamos National Laboratory, Los Alamos, NM

Eric R. Pardyjak, Joseph C. Klewicki
University of Utah, Salt Lake City, UT

1. INTRODUCTION

Understanding the turbulence characteristics of ASL flow in and through urban areas is essential to predicting dispersion in cities. Urban areas, however, alter the inherent turbulence found in the Atmospheric Surface Layer (ASL) through a variety of mechanisms. Due to the difficulty in obtaining characteristic measurements of the turbulence in actual urban areas, simplified models (usually wind tunnel models) are typically used to isolate the mechanisms affecting turbulence characteristics in and around buildings or groups of buildings. Results from these simplified models are often used to validate computational models. These models are in turn used to predict the turbulence and flow characteristics in actual urban areas that have complex geometries and topography based on a limited amount of data found in the urban area.

The depth of the ASL is typically much larger than most buildings making it possible to consider urban areas as surface roughness at large scales. At large scales the urban area therefore produces a flow regime above an urban area (in the inertial sublayer and above) that is basically an ASL flow that has been modified by the presence of the urban terrain below it. It can be argued that the flow regime transitions to a bluff body flow that is influenced by the upstream ASL conditions surrounding it through the Urban Roughness Sublayer (URSL) and into the Urban Canopy (UC). In these regimes it is rational to expect that the bluff body flow characteristics (i.e. wake and recirculation regions, vortex shedding, etc.) impose scales in the flow that affect the turbulence and transfer of energy between eddies of different sizes. Thus a detailed understanding of these phenomena is, for example, necessary to accurately validate high-resolution computational models.

This paper compares sonic anemometer data obtained in an actual urban area during the Joint Urban 2003 (JU03) Field Experiment with those data obtained in a simulated urban area during the Mock Urban Setting Test (MUST). JU03 was held in downtown Oklahoma City in a street canyon, while MUST was performed around an array of aligned, same-size obstacles simulating an urban area at near full scale. These experiments, both performed in a true ASL, provide an opportunity to compare turbulence and flow characteristics produced by an actual urban canyon with semi-complex geometry and those found in a simulated urban canyon with a highly simplified geometry.

Local effects were found to dominate the flow in the lowest 10% of the canyon, often producing predominantly positive along-wind to vertical cospecta and large variations in the mean turbulence statistics. A complicated flow structure was found in the canyon with large mean vertical velocity components. Local phenomena were found also found to dramatically affect the energy cascade in some cases by adding energy over discrete bandwidths or altering the slope of the spectra in the high frequency range from the typical $f^{-5/3}$ behavior of the inertial subrange.

2. EXPERIMENTAL DETAILS

2.1 *Joint Urban 2003*

The Joint Urban 2003 field campaign was performed from 29 June through 30 July 2003 in Oklahoma City (OKC), OK. OKC provided a relatively large urban area located in idealized terrain devoid of major topological features. A section of Park Avenue found in the urban core of OKC was selected to concentrate a large number of measurements in a single urban canyon. The average building height (H) for the selected urban canyon was ~50 m with a corresponding canyon width (W) of ~25 m and canyon length (L) of ~150 m, making H/W ~ 2. An analysis of the building data sets in the urban core of OKC performed by Burian et al. (2003) found the plan area fraction (λ_p) to be 0.35 and the frontal area index (λ_f) to range between 0.14 and 0.22 depending on wind direction. These values characterize the flow through the urban core as skimming flow using the thresholds suggested by Oke (1987).

Figure 1 shows the relative locations of the wind instruments deployed in the Park Avenue urban canyon. Forty-three 3D sonic anemometers were placed in and around the urban canyon, these sensors acquired nearly continuous data throughout the entire month of July, while during the 10 Intensive Observation Periods (IOP), when dispersion experiments were performed, an additional two 3D sonic anemometers and seven 2D sonic anemometers were deployed on tripods at the ends of the canyon.

**Corresponding author address:* Matthew A. Nelson, Los Alamos National Laboratory, Group D-4, MS K575, Los Alamos, NM 87545; e-mail: nelsonm@lanl.gov

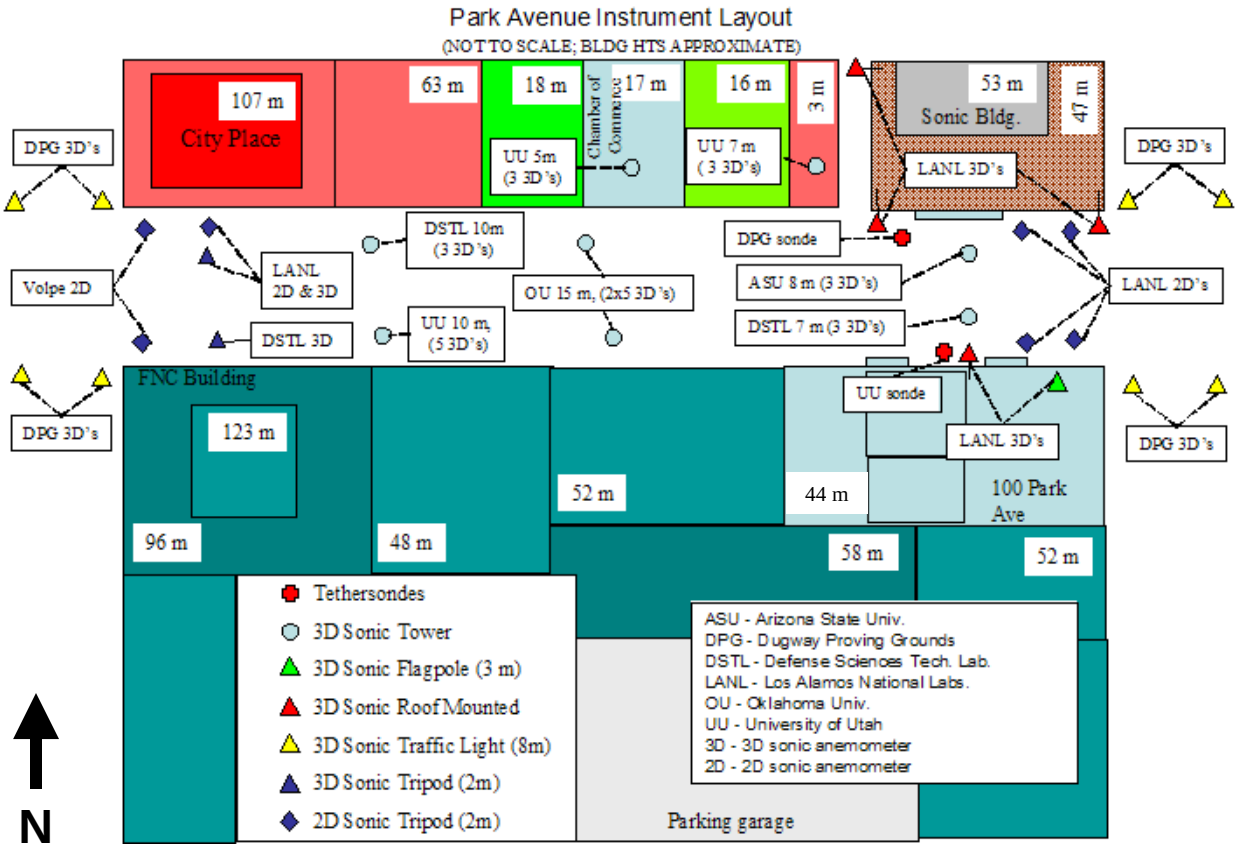

Figure 1. Schematic of the relative locations of the wind instrumentation on Park Avenue (not to scale) including the type of instrument and the organization responsible for its operation. Typical winds were southeasterly to southwesterly. Note the tall buildings on the west end of the street canyon and the low buildings in the center on north side of the canyon. LANL sonic 2 is located on the overhang of the building at the southeast corner of the canyon. LANL sonic 3 and 4 are located on the northwest and southwest corners of the building at the northeast corner of the canyon. LANL sonic 5 is located on the flagpole on the building at the southeast corner of the canyon.

The inherent unsteadiness found in ASL flow makes obtaining meaningful statistical results difficult in the most ideal conditions; the complicated geometries found in urban areas act to exacerbate these difficulties. In order to obtain meaningful results from statistical tools it is necessary to find time periods where the flow is quasi-steady in the mean. Typical winds during JU03 were southeasterly to southwesterly. Most of the data presented here has been extracted from IOP 10 (0130 to 0300 CDT on 29 July 2003) due to the relatively steady flow conditions during this time period. The upstream winds, as measured by the Pacific Northwest National Laboratory (PNNL) SODAR, were oblique to the orientation of Park Avenue, gradually shifting from a bearing of 212 to 222 during this time period, causing a channeling flow regime to develop in the urban canyon and creating quasi-static mean flow features to form. While a vehicle traffic experiment was concluded 15 minutes prior to this time period, there was negligible traffic in the canyon during the selected time period. This isolates the local effects found in the base of the canyon to turbulence generated from flow over stationary objects. Thus leaving the time periods experiencing traffic induced turbulence for future analysis.

Figures 2-5 are photographs of some of the locations of the sonic anemometers within and above the Park Avenue urban canyon. Various obstacles exist at the base of the canyon such as trees, statues, cars (both moving and stationary), etc. These further complicate the flow at street level. There are also deviations in the canyon geometry from the idealized urban canyon. The building heights shown in Figure 1 indicate that the two buildings at the west end of the canyon are significantly taller than the rest of the buildings along the canyon walls. There was also a section of buildings along the middle of the north side of the canyon that were significantly shorter than the rest of the buildings comprising the canyon. Both features will cause deviations from the ideal urban canyon depending on the wind direction.

Figure 2. Photograph of the Park Avenue urban canyon taken from the roof of the building at the northeast corner of the street canyon looking west. Several towers with multiple 3D sonic anemometers are visible in the canyon. Note the various obstacles at street level which will produce localized effects on the flow.

Figure 3. Photograph of the Park Avenue urban canyon taken at street level from the east end of the canyon looking west.

2.2 *Mock Urban Setting Test (MUST)*

MUST was performed during the month of September 2001 in Utah's West Desert at the US Army Dugway Proving Ground (DPG), Biltoft (2001). MUST consisted of 120 shipping containers set into a 10 by 12 aligned array placed on relatively flat terrain vegetated by low shrubbery as seen in Figure 6. Each shipping container was 12.2 m long, 2.42 m wide, and 2.54 m high (*H*). The average spacing between the obstacles parallel to the length was 7.9 m and the average spacing perpendicular to the length was 12.9 m. This gives a λ_p of 0.096 and λ_f of 0.10 and 0.03 using the length and width, respectively, canyon aspect ratios *H/W* and *H/L* of 0.20 and 0.21 respectively, Yee and Biltoft (2004). Using the thresholds suggested by Oke (1987), this geometry produces isolated roughness regime flow. As such the interaction between individual obstacles will be different in the MUST array than the interaction between individual buildings in JU03.

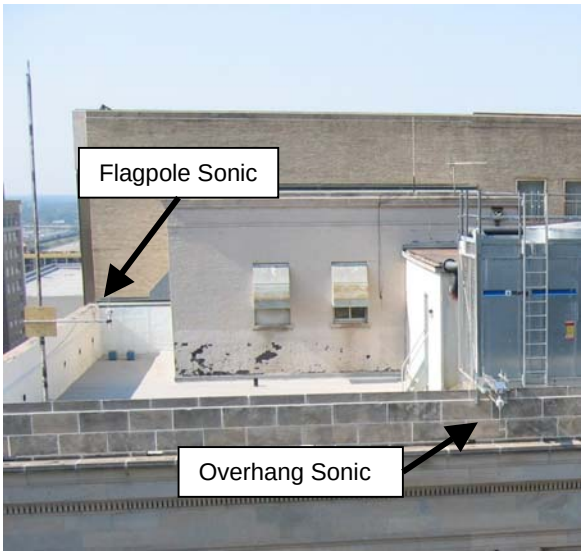

Figure 4. Photograph of the two 3D sonic anemometers located on the building at the southeast corner of the Park Avenue urban canyon taken from the roof of the building at the northeast corner of the canyon. One sonic anemometer is mounted to the flagpole on the left of the picture and the other is mounted over the side of the building and is on the right in the photograph.

Figure 5. Photograph of the building located at the northeast corner of the Park Avenue urban canyon taken from the middle of the canyon at street level. A single 3D sonic anemometer is located on each of the visible corners of the building.

Various 2D and 3D sonic anemometers were placed around, above, and throughout the array on various towers (see Figure 7). Several sonic anemometers were deployed in the southern-most canyon of the MUST array (see Figure 8) in order to provide as detailed information in the canyon as possible. The data taken in the southern-most canyon of the MUST array were chosen for comparison with the real urban canyon flow. Further

Figure 6. Photograph of the MUST array taken from the southeast corner of the array looking west (courtesy of C.A. Biltoft DPG, ret.).

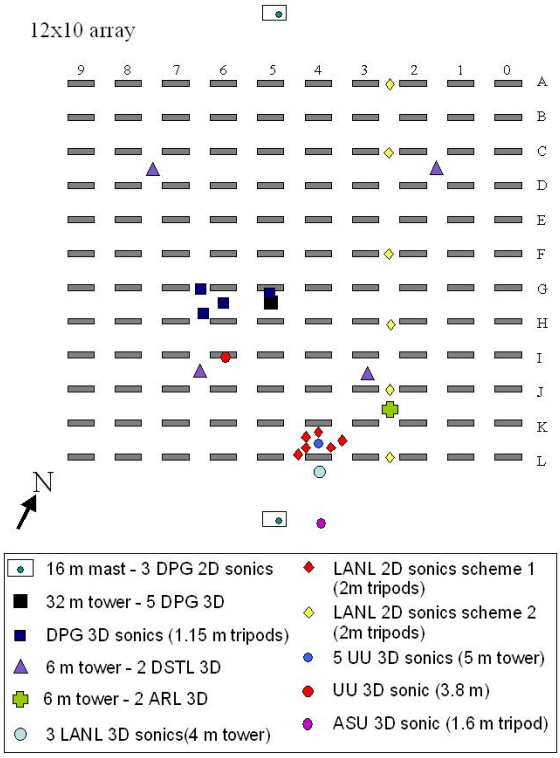

Figure 7. Schematic of the sonic anemometers deployed in MUST with their relative locations within the array. This manuscript focuses on the data obtained in the center of the urban canyon at the bottom of the diagram. LANL 2D sonic scheme 1 was deployed on 20 September 2001 and after, while scheme 2 was deployed before that time. The schematic is not to scale.

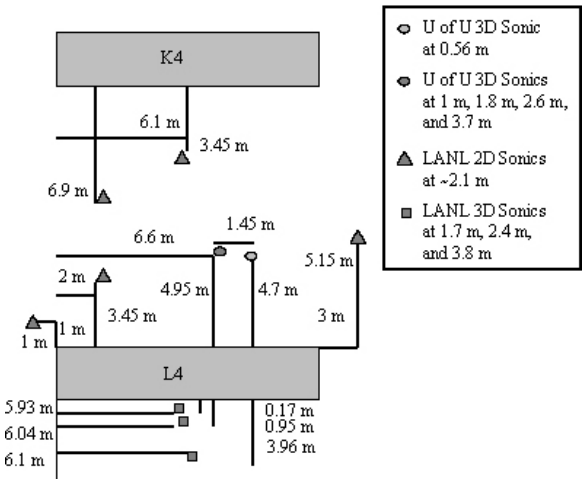

Figure 8. Close up view of the southern-most canyon of the MUST array with distances relative to the two containers forming the canyon. LANL 2D sonics deployed in the positions shown on 21 September 2001 and after. The schematic is not to scale.

information on some of the other sonic anemometers employed in the MUST array can be found in Nelson et al. (2004 a and b).

During the time period between 2305 and 2335 MDT on 13 September 2001, steady northerly winds caused the southern-most canyon of the MUST array to experience well-developed flow, approximately 35° oblique to the array. These conditions promoted minimal entrance and alignment effects within the array.

3. RESULTS

The heat storage capacity in the urban core of OKC is much greater than that of the containers used in MUST and as such it was not possible to completely match the stability conditions between the two cases. Nevertheless, periods of time were selected from both data sets with relatively steady wind conditions and with stability conditions as similar as possible.

The basic assumptions used to derive standard ASL similarity theory are certainly not met within the UC. This poses a problem since a true similarity theory has yet to be developed for urban areas. Due to the complexity of true urban flows with numerous imposed scales, it is difficult to determine the characteristic flow scales. In the absence of a similarity theory for urban areas, if the quantities that are typically used in ASL similarity theory are viewed as a local measure of various turbulence parameters some of the analyses and comparisons found in similarity theory may still prove useful. As such a velocity scale (V_*) is defined as:

$$V_* = \left(\overline{u'w'}^2 + \overline{v'w'}^2 \right)^{1/4} \quad (1)$$

This velocity scale should not be confused with the shear velocity (u_*) even though it is computed in the

same manner but should be viewed with its relation to the local average Reynolds shear stress. A length scale (L_l) can be computed using this velocity scale and the vertical turbulent heat flux:

$$L_l = \frac{-\overline{\theta} V_*^3}{\kappa g \overline{w'\theta'}} \quad (2)$$

Again this length scale should not be confused with the characteristic Monin-Obukhov length from ASL similarity theory. In this case a local stability parameter (z/L_l) is formed that can be computed by a single 3D sonic anemometer, where z is the height above ground level. This stability parameter is closely related to the flux Richardson number, which is the ratio of the buoyancy production/destruction term to the shear production term of the turbulent kinetic energy (TKE) equation. A negative vertical turbulent heat flux corresponds to a positive L_l and is indicative of thermally stable conditions, while a positive vertical turbulent heat flux corresponds to a negative L_l and thermally unstable conditions.

3.1 *Joint Urban 2003 Mean Turbulence Statistics*

Figure 9 is an example time series of the along canyon wind (u), cross-canyon wind (v), vertical wind (w), and temperature (T) from the sonic anemometer at z = 9.84 m on the University of Utah (UU) tower located at the west end of the Park Avenue canyon (see Figure 1). With exception of the temperature the time series are steady in the mean. The time series shows a positive u component and a v component that fluctuates about zero, indicating westerly channeling. Recall that during this time the winds aloft are southwesterly. In order to obtain meaningful fluctuating temperatures a 15-minute running mean was employed. The statistics presented are computed using the entire hour and a half of data.

Figures 10-12 are vertical profiles of wind speed, direction, and mean vertical velocity, respectively, produced by some of the sonic anemometers within the Park Avenue urban canyon. Note that the street level sonic anemometers from Los Alamos National

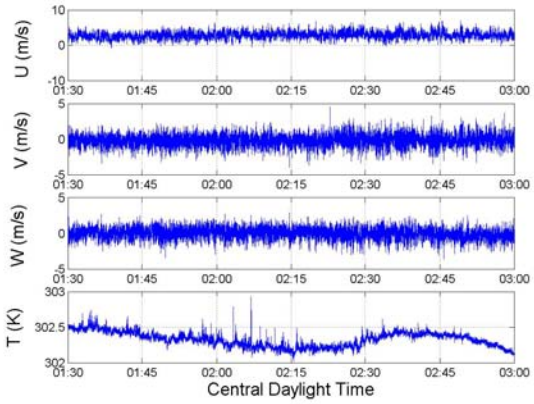

Figure 9. JU03 Time series from 0130 to 0300 29 July 2003 CDT from the UU sonic anemometer at z = 9.84 m.

Laboratory (LANL) sonic 1, the UU tower, the north University of Oklahoma (OU1) tower, the south OU tower (OU2), and the Arizona State University (ASU) tower are positioned from west to east down Park Avenue (see Figure 1). The other four LANL sonic anemometers are located at the east end of the canyon at roof level. LANL sonic 2 is located on the overhang of the building at the southeast corner of the canyon. LANL sonic 3 and 4 are located on the northwest and southwest corners of the building at the northeast corner of the canyon. LANL sonic 5 is located on the flagpole on the building at the southeast corner of the canyon. It should be noted that the sonic anemometers on OU2 were found to occasionally have some problems with the data, as such the data reported for the 15 m sonic on OU2 was obtained only from the time period of 0230 to 0300 29 July 2003 CDT.

Figure 10 shows that the flow decelerates as it travels down the canyon. An inflection point is present in the wind speed profiles produced by three of the towers. Local effects appear to dominate flow characteristics at the bottom of the canyon. The wind directions indicate that, with a few exceptions, the along-canyon component of the velocity is dominant. LANL sonic 3 is located at the northwest corner of the building at the northeast corner of the canyon. At this location the prevailing flow has been deflected by the west side of the building causing the cross-canyon component to dominate the flow in this region. The ASU tower has trees in close proximity to the east and west (shown in the right hand side of Figure 3), which dramatically affect the flow in this region; causing a significant reduction in flow speed and possibly deflected in the direction as well. It can be seen in Figure 4 that with the southwesterly prevailing winds LANL sonic 5 was in the wake of the buildings upstream, which will obviously dominate flow features in the immediate region.

The mean vertical velocities shown in Figure 12 demonstrate some of the complicated flow structures present in the canyon due to the oblique upwind flow. Significant vertical velocities are found throughout the canyon with the strongest found on the leeward side of the southeast building by LANL sonic 2. One would typically expect to find positive vertical velocities on the southern wall and negative vertical velocities on the northern wall due to the southerly component of the prevailing winds. The vertical velocities from OU1 and OU2 show that the opposite is true at the center of the canyon. In general the same is true throughout the canyon with the measurements made on the southern side of the canyon yielding predominantly negative vertical velocities and predominantly positive vertical velocities on the northern side of the canyon. This may be evidence of “corkscrew” flow in the canyon as suggested by Nakamura and Oke (1988), however, there are insufficient measurements to be conclusive.

Figure 13 shows that the TKE tends to decrease throughout the canyon near street level. The roof-level sonic anemometers on the northeast

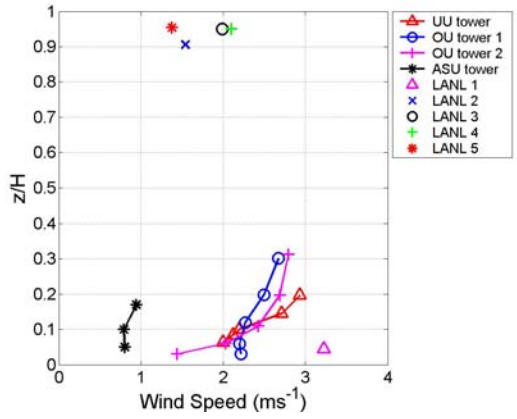

Figure 10. JU03 wind speed profiles within the Park Avenue canyon.

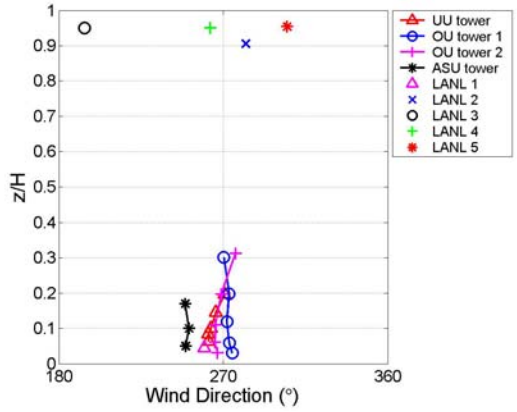

Figure 11. JU03 wind direction profiles within the Park Avenue canyon.

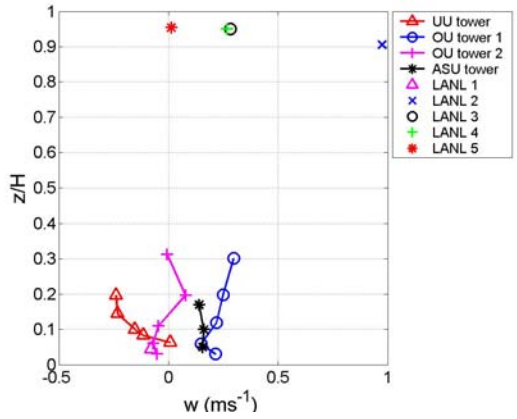

Figure 12. JU03 mean vertical velocities measured throughout the Park Avenue Urban canyon.

building have the highest TKE, while the roof top sonic anemometers on the southeast building have relatively low TKE. It can be seen in Figure 4 that the buildings immediately upstream of the sonic anemometers on the southeast building are several meters taller than the southeast building. As such these sonic anemometers will not experience the strong shear found between the flow above and below average building height. The sonic anemometers on the northeast building are more likely to be located within this region of high shear. Results from numerous other experiments of real and artificial urban roughness such as Kastner-Klein and Rotach (2004), Cheng and Castro (2002 a and b), Hanna et al (2002), and Rotach (1999) have shown that maximum TKE and related values such as r.m.s velocities and Reynolds stresses typically occur just above the average building height. The results from the sonic anemometers on the northeast building, which have the fewest localized effects, suggest that the same is true of the measurements made in the Park Avenue canyon.

Figure 14 is the plot of the Reynolds shear stress velocity scale (V_*) measured by the various sonic anemometers within the canyon. Note that V_* varies significantly with height and lateral location in the canyon, indicating that the traditional u_*-based scaling approach may not be possible, i.e., it is unclear which u_* is characteristic of the flow throughout the canyon. The measurements show that, as was found in TKE, the roof level sonic anemometers with the fewest localized effects exhibit the maximum value in the canyon. The trend of increasing V_* with height also agrees with the results of the above-mentioned experiments. The local effects also appear to dominate the character of the flow at the base of the canyon causing large variability in V_* as measured by the lowest sonic anemometers in the canyon.

The local stability parameter (z/L_l) measured throughout the canyon is shown in Figure 15. Even though the time period selected is in the middle of the night (0130 to 0300 CDT), the only regions with positive (z/L_l) are found at some of the roof level sonic anemometers. The sonic anemometers throughout much of the lowest 10% of the canyon exhibit relatively strong instability (compared with other regions within the canyon) long after sunset. Local effects appear to also have a dramatic effect on the stability as evidenced by the two OU towers located at the center of the canyon. Although the two towers are located more or less directly across the street from each other, they experience very different thermal conditions. These results demonstrate the difficulty in determining characteristic scales within the canyon.

Figure 16 is a comparison of the standard deviations of the along-canyon, cross-canyon, and vertical components of velocity normalized by V_* measured in the canyon with the typical neutral ASL standard deviations of along-wind, cross-wind, and vertical velocity components normalized by V_*, which in the case of the neutral ASL should be the same as

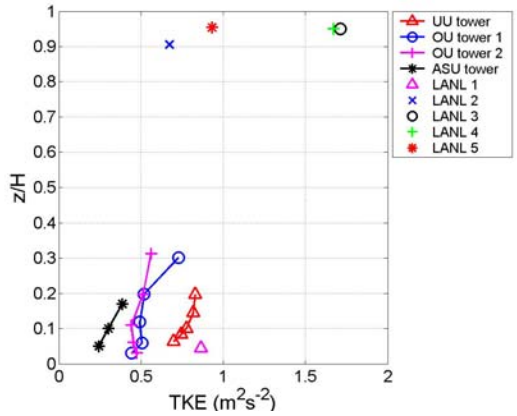

Figure 13. JU03 turbulent kinetic energy profiles within the Park Avenue canyon.

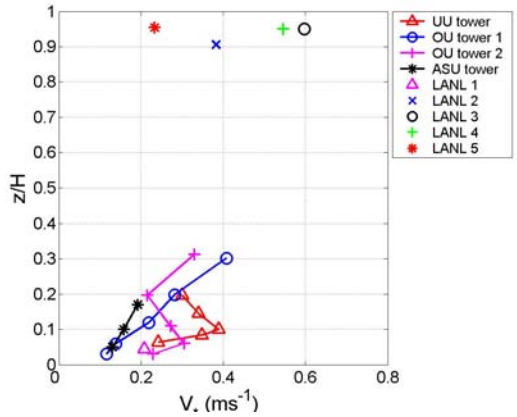

Figure 14. JU03 Reynolds shear stress velocity scale profiles within the Park Avenue canyon.

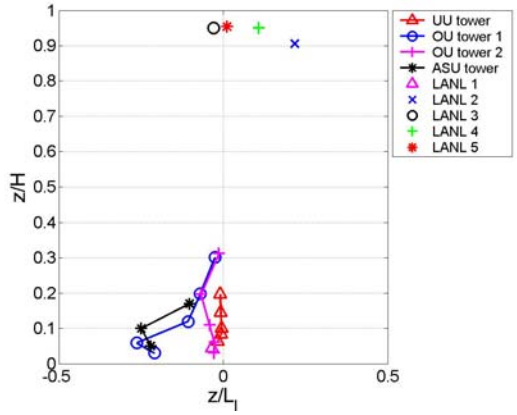

Figure 15. JU03 local stability parameter profiles within the Park Avenue canyon.

u_*. Note that the cross-canyon component is dominant for LANL 3 and LANL 5 is located in the wake of the buildings upstream and should therefore not be expected to exhibit the same properties as the other sonic anemometers. The largest deviations from typical ASL values generally occur in the sonic anemometers closest to street level, as such the velocity fluctuations in the lowest 10% of the canyon are large compared to the local vertical transport of horizontal momentum. Most of the sonic anemometers above the lowest 10% of the canyon have fluctuating velocity to V_* ratios closer to those found in the ASL. Comparing the trends seen in V_* from Figure 14 with the fluctuating velocity to V_* ratios seen in Figure 16, it can be seen that the decreasing trends with height seen in Figure 16 are likely due at least in part to the opposite trend seen in Figure 14. This argues for something other than purely local scaling.

A common practice is to normalize by quantities in the region of maximum shear stress, e.g. Kastner-Klein and Rotach (2004) and Rotach (1999). Using the V_* from LANL sonic 4 as a reference velocity scale throughout the entire canyon produces the results seen in Figure 17. This type of normalization makes the relative magnitudes of the fluctuating velocity components become apparent. The fluctuations in the along-canyon component u remain more or less constant with height but decrease slightly with downwind distance into the canyon. Fluctuations in the cross-canyon component v and the vertical component w both tend to decrease with downwind distance in the canyon and increase with height in the canyon interior. It is also apparent that V_* increases with height more rapidly than the fluctuations in velocity, which caused the trends in Figure 16 to opposite to those found in the fluctuating velocities. A compromise between the two methods may be more appropriate for the following three reasons: first, local effects are still evident, the amount of interaction between the Reynolds shear stress at building height and the local fluctuations in velocity is unknown, and third, Figure 15 shows that the local stability measured at building height is not characteristic of the canyon interior flow.

The sonic anemometers at the top of the towers tended to exhibit fluctuating velocity to V_* ratios closer to those found in the neutral ASL. If the V_* values measured at the top of each tower are used as a quasi-local velocity scale to normalize the other data on the same tower the plots found in Figure 18 are produced. Using the quasi-local normalization the ratios for the tower sonic anemometers are closer to the ratios found in the ASL. The vertical ratios are closest to the ASL on the OU towers, which are 50% taller than all the other towers in the canyon. A local value above the lowest 10% of the canyon where small-scale local effects are strongest should sense the larger-scale local effects found throughout the canyon while minimizing the small-scale local effects due to phenomena in the immediate vicinity of the tower.

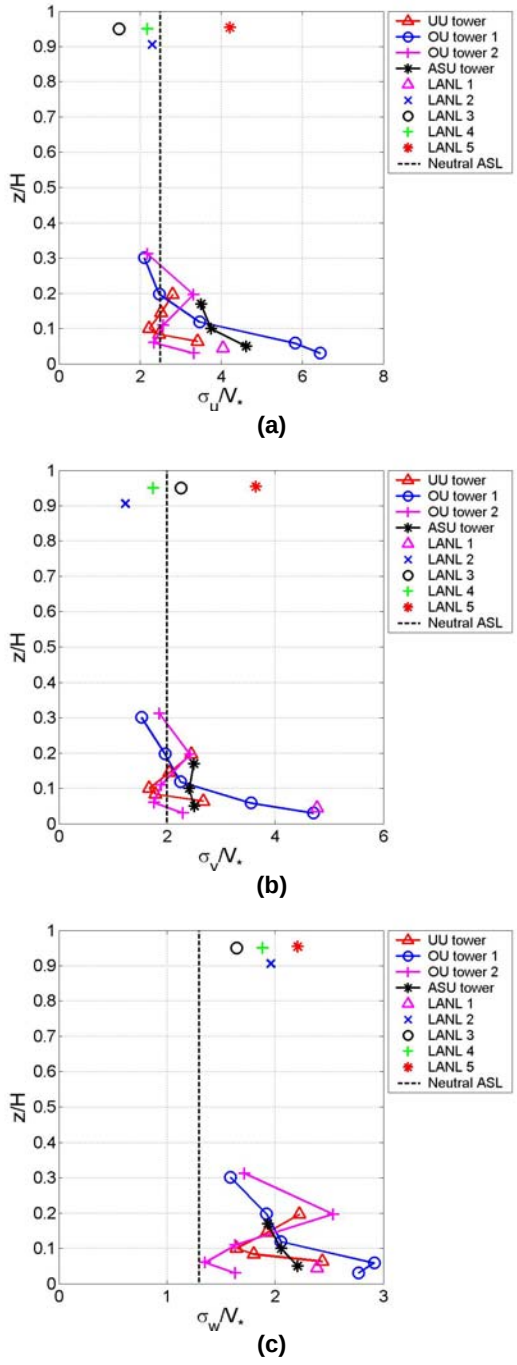

Figure 16. JU03 comparison of the along-canyon (a), cross-canyon (b), and vertical (c) fluctuating velocity components normalized by the Reynolds shear stress velocity scale compared with neutral ASL similarity theory.

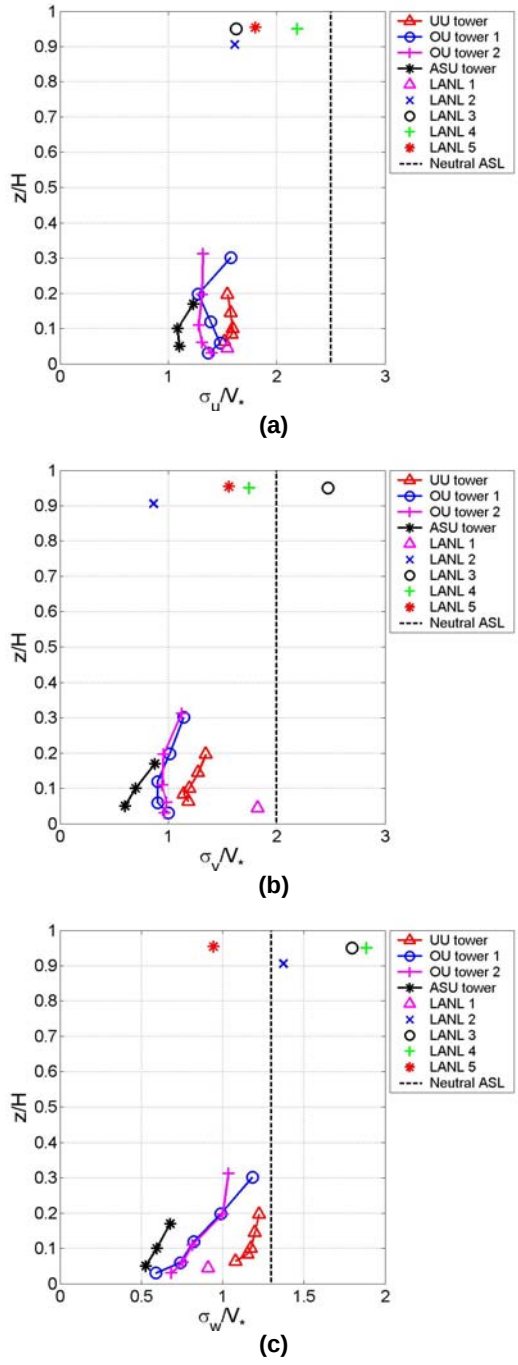

Figure 17. JU03 comparison of the along-canyon (a), cross-canyon (b), and vertical (c) fluctuating velocity components normalized by the Reynolds shear stress velocity scale measured by LANL sonic 4 compared with neutral ASL similarity theory.

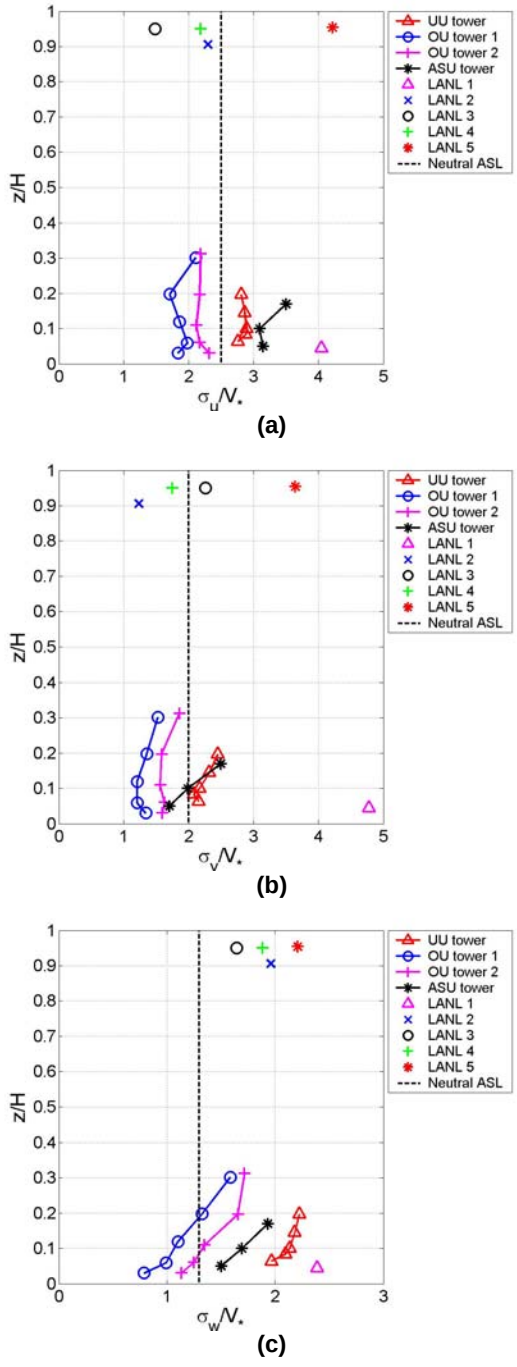

Figure 18. JU03 comparison of the along-canyon (a), cross-canyon (b), and vertical (c) fluctuating velocity components normalized by the Reynolds shear stress velocity scale compared with neutral ASL similarity theory. Quasi-local Reynolds shear stress velocity scale measured at the top of each tower used to normalize the all the sonic anemometers on the tower.

3.2 *MUST Mean Turbulence Statistics*

The standard meteorological velocity convention time series for the half hour of data selected from the MUST experiment taken from the UU sonic anemometer at z = 3.7 m (z/H = 1.46) are shown in Figure 19. These example time series are presented to demonstrate the steady character of the flow. A 15-minute linear detrending scheme was used to produce the fluctuating time series and the flow was rotated into the local mean wind for each of the sonic anemometers with the along-wind component (u), the cross-wind component (v), and the vertical component (w). The statistics presented are calculated using the entire half hour record. Note that the selected time period was acquired under northerly wind conditions, and thus, the lower two LANL sonic anemometers were located in the wake of container L4 (see Figure 8), while the sonic anemometers above obstacle height H are both located in a well developed RSL.

Figures 20-22 present the local wind speed, direction, and mean vertical velocity, respectively. These were measured within and downstream of the southern-most canyon of MUST. The wind speed profile acquired by the LANL tower is complicated due to the fact that the sonic anemometers are not located at the same horizontal position relative to the container. The sonic near building height is much closer to the obstacle than the lowest sonic, and thus the local obstacle effects are more intense. While the sonic located at z/H = 0.22 is the only sonic found to exhibit full recirculating flow conditions, the other sonic anemometers below building height exhibit some slight channeling effects adding a slight easterly component to the flow that increases with distance below building height in the canyon. The vertical velocities from the UU tower show that there is very little mean vertical movement at the center of the canyon, while the LANL sonic anemometers at 3.8 m and 1.7 m show significant down drafts in the wake of container L4.

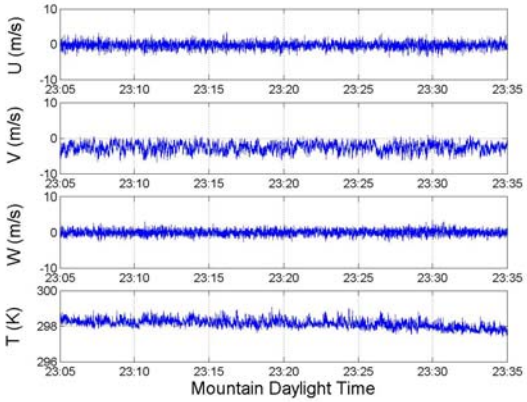

Figure 19. MUST 20 Hz time series from 23:05 to 23:35 on 9/13/2001 MDT from UU sonic anemometer at z = 3.7 m using standard meteorological coordinates.

Figure 23 shows that the TKE in and around the simulated canyon exhibits very similar behavior to the wind speed shown in Figure 20. Nelson et al (2004b) shows that the maximum TKE in the MUST was found to occur at levels near building height. Again agreeing with the data from the various other experiments such as Kastner-Klein and Rotach (2004), Cheng and Castro (2002 a and b), Hanna et al (2002), Rotach (1999). Figure 24 shows a different trend in V_* than is found in TKE for the LANL tower. While the building height sonic on the LANL tower measured the lowest values of both TKE and V_*, the lowest level exhibits the maximum V_* on the tower, which is completely opposite to the trends found in JU03 presented in Figure 14.

The thermal stability within the MUST array has very different characteristics from those found in JU03 (see Figures 15 and 25). While several sonic anemometers were found to have near neutral stability in JU03, only some of the roof level sonic anemometers were found to have positive z/L_l. All of the sonic anemometers in MUST measured a positive z/L_l over the selected time period. As opposed to the tendency for more thermally unstable conditions found in JU03, the sonic anemometers in the MUST canopy exhibit a tendency towards more thermally stable conditions. Local obstacle effects on stability are evident in comparing the stabilities measured with the canyon by the UU sonic anemometers that are several meters away from the nearest building with those measured by the LANL sonic anemometers at the same level that are located closer to the containers. The LANL sonic anemometer located at building height in the wake of container L4 measured the most neutrally stable conditions while the UU sonic anemometer at building height less than 10 m away measured z/L_l to be larger by a factor of 4. The stability parameter z/L_l maintains a nearly constant value across the RSL. While one might expect the RSL to be more homogeneous than the canopy, it is far from homogenous as is evidenced by the differences in other measures of turbulence between the two sonic anemometers.

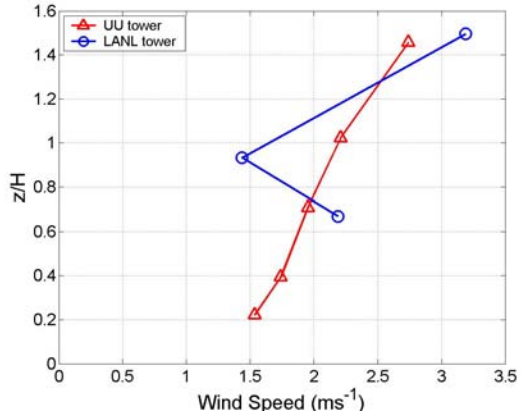

Figure 20. MUST wind speed profiles within (UU) and downstream (LANL) of the southern-most canyon.

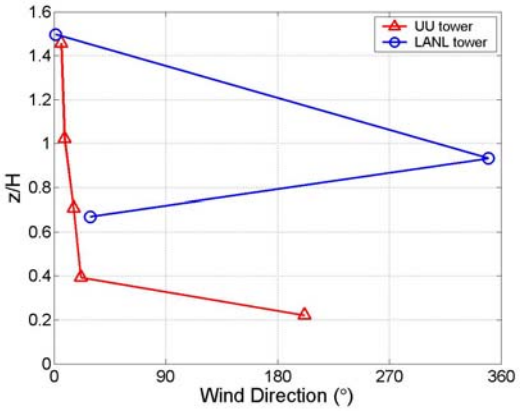

Figure 21. MUST wind direction profiles within (UU) and downstream (LANL) of the southern-most canyon.

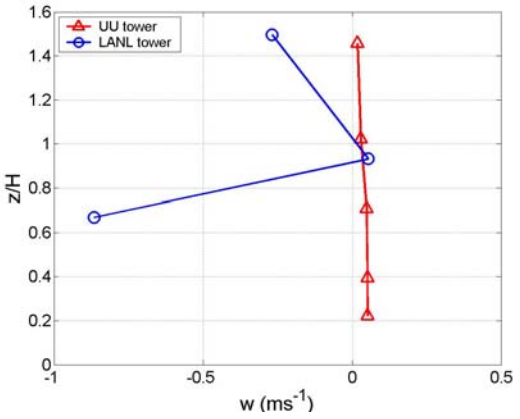

Figure 22. MUST mean vertical velocities measured within (UU) and downstream (LANL) of the southern-most canyon.

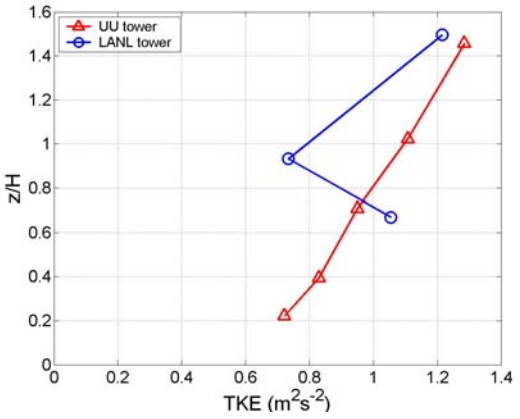

Figure 23. MUST turbulent kinetic energy profiles within (UU) and downstream (LANL) of the southern-most canyon.

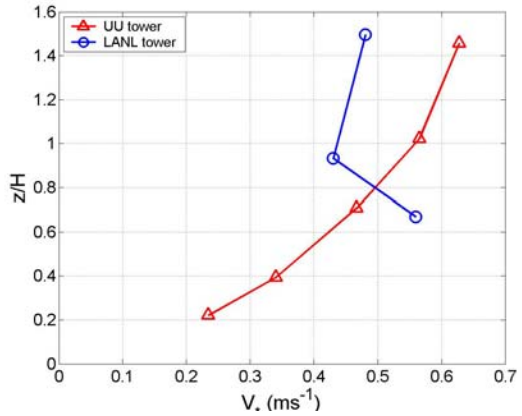

Figure 24. MUST Reynolds shear stress velocity scale profiles within (UU) and downstream (LANL) of the southern-most canyon.

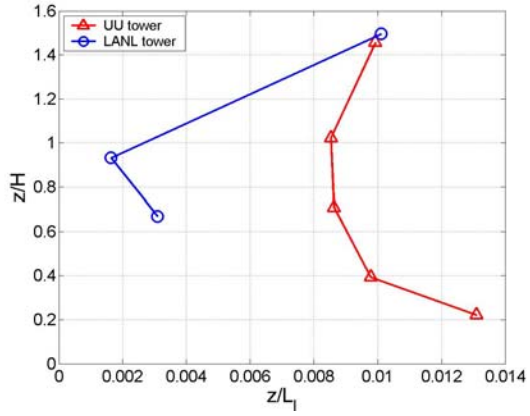

Figure 25. MUST stability parameter profiles within (UU) and downstream (LANL) of the southern-most canyon.

Similar to the results found in JU03 the ratio of the fluctuating velocity components to V_* were found to be much higher than the values from the neutral ASL near the bottom of the canyon and decrease with increasing z (see Figure 26). As seen in Figure 24, the V_* follows the same trend in the canyon that was seen in the JU03 data, thus the trend in V_* will have a similar effect on the fluctuating velocity ratios, however, using the fully local ratios with the MUST data produces values that are more similar to the ASL values than it did with the JU03 data (see Figure 16). The V_* measured at the top of each tower (in the RSL) are used to normalize fluctuating velocities in Figure 27. This may not be an appropriate normalization in the case of the LANL tower since the sonic anemometers are not located in the same horizontal position relative to the obstacle and as such local effects have been enhanced. However, the magnitudes of the fluctuating velocities relative to the other values on the same tower are evident in these plots. The along-wind and vertical component fluctuations are seen to increase monotonically with height on the UU tower. The cross-wind component fluctuations are nearly constant on the UU tower. The local effects due to the proximity of the obstacle are evident in the obstacle height sonic on the LANL tower. Nelson et al. (2004b) found that the ASL flow characteristics aloft influenced obstacle induced flow features within the array. One might expect there to be a stronger interaction between the flow characteristics in the canopy of the MUST array than was found in the UC in the JU03 data for a couple of reasons: First, the area fraction for the MUST array was much lower than it was in the urban core of OKC, thus the flow aloft is more likely to permeate into the canopy. Second, the obstacle height in MUST is much smaller in relation to the ASL height than is the building height in JU03. Since a stronger interaction between the flow aloft and the obstacle induced flow is likely to exist, normalization with a V_* measured aloft may be the most appropriate for the MUST array. Unfortunately the sonic anemometers located on the Dugway Proving Ground 32 m tower at the center of the array (see Figure 7) were not operational during the selected time period.

3.3 *Joint Urban 2003 Spectra*

The power spectra energy density (PSD) and cospectral energy density as measured by the 3D sonic anemometers within and above the urban canyon provide information as to the important length and times scales and how energy is transferred between the eddies of various scales in the canyon. Due to the inherent inhomogeneity found in urban landscapes the spectra from different locations within the canyon have characteristics distinct from each other. Imposed flow scales generally result in spikes in the spectra at the corresponding frequency.

In order to produce the spectra from the same JU03 data presented in Section 3.1, the fluctuating components of the wind were determined using a 15-minute running-mean detrending scheme. As such u is the component of the wind vector aligned with the canyon, v is the cross-canyon component, and w is the vertical component. A 10-minute window was used to produce the spectra, and the resulting spectra were smoothed using an 11 data point running-mean. All spectra have been normalized by V_* and plotted versus frequency normalized by z and the local horizontal wind speed U. Characteristic inertial subrange behavior ($f^{-5/3}$ for non-premultiplied spectra and $f^{-2/3}$ for premultiplied spectra) is indicated on PSD plots for comparison with Kolmogorov energy cascade-like behavior.

Figure 28 shows the along-canyon and vertical premultiplied PSD as well as the along canyon to vertical cosprectrum from the LANL 3D sonic anemometer located at z = 2.2 m at the west end of the Park Avenue canyon. Figures 28a and c show that the high frequency range of the PSD of both the along-canyon and vertical components of velocity do not exhibit typical $f^{-2/3}$ inertial subrange behavior but

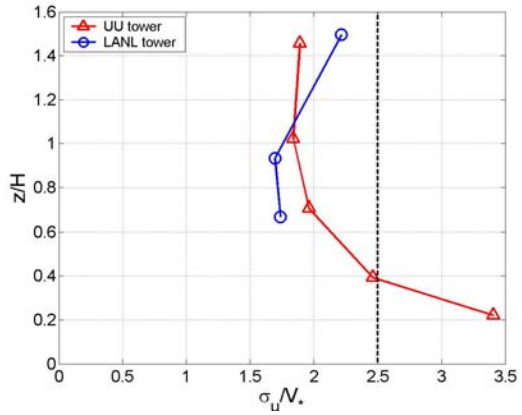

(a)

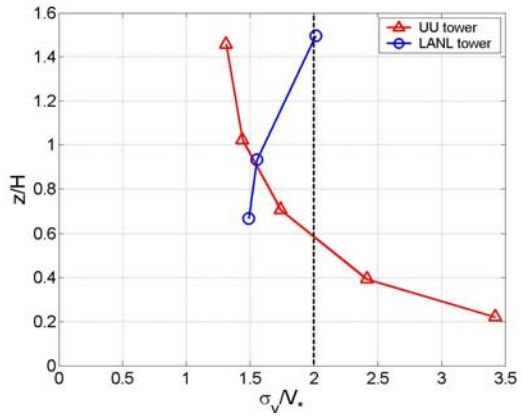

(b)

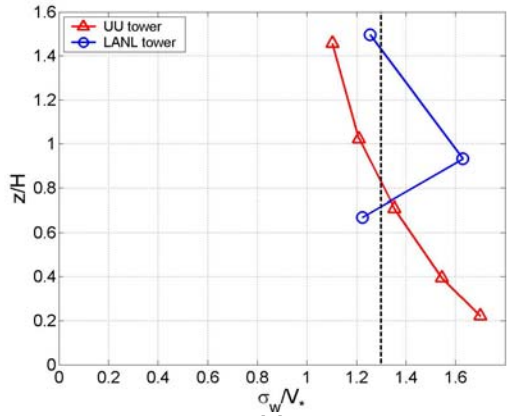

(c)

Figure 26. MUST comparison of the along-wind (a), cross-wind (b), and vertical (c) fluctuating velocity components normalized by the Reynolds shear stress velocity scale compared with neutral ASL similarity theory within (UU) and downstream (LANL) of the southern-most canyon.

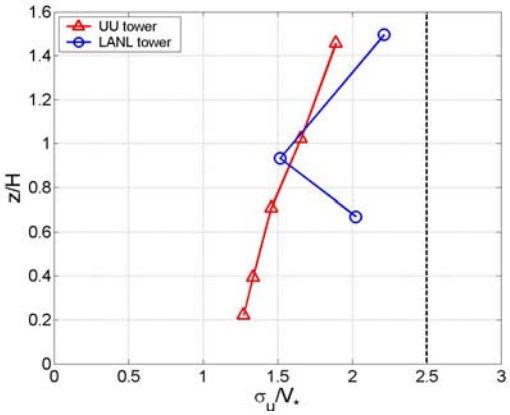

(a)

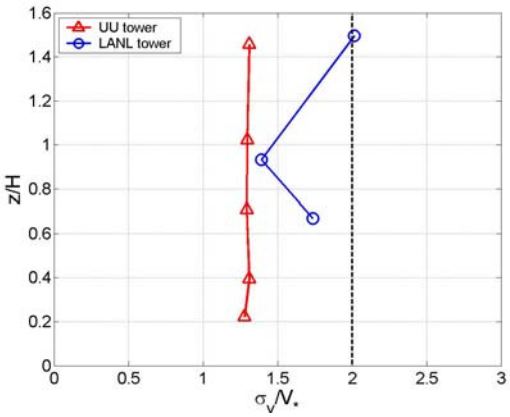

(b)

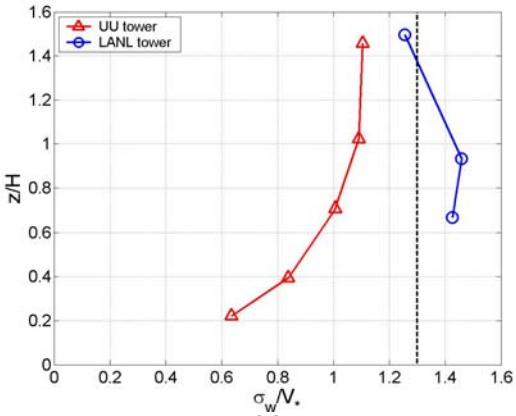

(c)

Figure 27. MUST comparison of the along-wind (a), cross-wind (b), and vertical (c) fluctuating velocity components normalized by the Reynolds shear stress velocity scale measured in the RSL of each tower compared with neutral ASL similarity theory within (UU) and downstream (LANL) of the southern-most canyon.

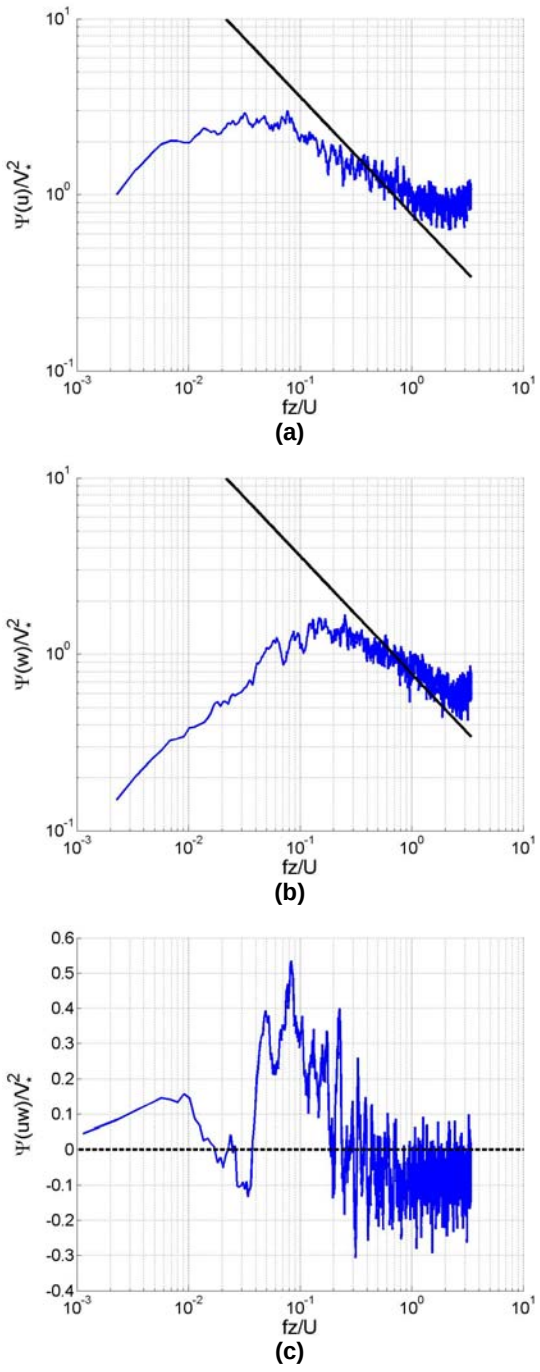

Figure 28. JU03 premultiplied spectra obtained from the LANL sonic at z = 2.2 m at the west end of the canyon (a) along canyon PSD, (b) vertical PSD, and (c) along canyon-vertical cosprectrum. The black line in (a) and (b) is to indicate the $f^{-2/3}$ slope characteristic of the inertial subrange.

instead follow something close to an $f^{-1/3}$ slope. The along-wind PSD has a small f^{-1} region (if plotted non-premultiplied) in the low to intermediate range of frequencies Figure 28c shows that the cosprectrum is predominantly positive peaking near fz/U = 0.1. This is opposite to typical ASL behavior.

Figure 29 shows the non-premultilied spectra from the z = 9.84 m level of the UU tower located on the south side of the street towards the west end of the canyon (see Figure 1). This plot demonstrates an unusual phenomenon that is found on all levels of the tower, the inertial subrange portion of the PSD remains constant for a short band of frequencies. Some turbulent process is adding energy into the flow in this region of the canyon at all heights measured by the sonic anemometers on the UU tower.

Figures 30-34 are premultiplied spectra from all of the sonic anemometers on the UU tower. When the PSD is premultiplied, the band of constant PSD appears to be a large spike in the spectra in the inertial subrange. This energy production occurs at length scales of approximately 1 to 5 m, which does not correspond to a major geometric feature of the canyon such as the canyon width. For this flow this energy is added into the frequency range that corresponds to the inertial subrange. These scales roughly correspond to length scales associated with vehicle traffic; however, the vehicle traffic should have had negligible effects as was discussed in Section 2.1. This plateau in the PSD appears to be present in all the data from the UU Park Avenue tower regardless of the upwind speed and direction. This phenomenon also occurs in the temperature PSD as measured by both the sonic anemometer and an accompanying fine-wire thermocouple. The temperature spectra are not shown in this manuscript. Surface turbulence sources would be expected to have a diminishing effect with z, which is not seen in the data. Tower oscillations would be expected to increase with z where the oscillations would be stronger, which is not evident in the data either. Also

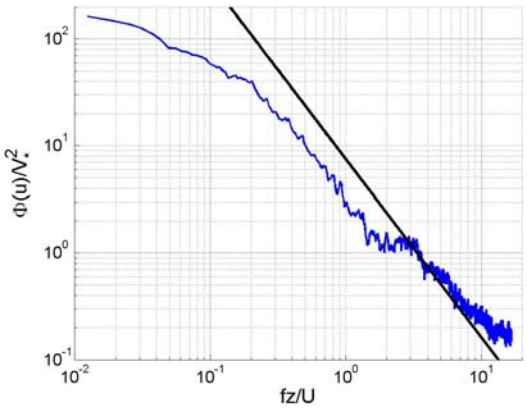

Figure 29. JU03 non-premultiplied along-canyon PSD obtained from the UU sonic at z = 9.84 m. The black line is to indicate the $f^{-5/3}$ slope characteristic of the inertial subrange.

this tower was not noted to be any less stable than any of the other towers in the canyon. The mean statistics measured from these sonic anemometers shown in Section 3.1 have reasonable values compared with the other sonic anemometers in the canyon and these sensors were also used in MUST and this phenomena is not found in the UU tower spectra that will be shown in Section 3.4, suggesting that this is not an instrument problem. To date, a conclusive explanation has yet to be found for this phenomenon.

The lower levels of the UU tower do exhibit some other strange behavior in the cosprectrum, with some scales where the cosprectrum is predominately positive, similar to the behavior of LANL sonic 1. This feature is more pronounced in the data obtained from OU1 on the north side of the street in the middle of the canyon (see Figure 1). The spectra obtained from the sonic anemometers on OU1 are seen in Figures 35-39. The spectra obtained from OU2, which is located on the south side of the street in the middle of the canyon is found in Figures 40-44. The PSD obtained from the OU towers exhibit the $f^{-2/3}$ inertial subrange behavior in the high frequency range of the PSD at all heights. The lowest sonics (at 1.5 m) on the OU towers are less than half the height of the lowest UU sonic (at 3.19 m). The cosprectrum is predominantly positive over the entire range of frequencies on the lowest level of OU1 (see Figure 35c), while the cosprectrum is positive only in the lowest frequencies measured by the lowest sonic on OU2 (see Figure 40c). The OU12.96 m sonic anemometer's cosprectrum (see Figure 36c) show that, while the lowest frequencies have changed from being positive to negative, there is still a range of intermediate frequencies that are positive before reaching the highest frequencies where the cosprectrum tends towards zero. At the OU1 5.97 m sonic a positive jump is seen in the cosprectrum at intermediate frequencies (see Figure 37c) but the cosprectrum does not actually become positive like it did at 2.96 m. This jump becomes less pronounced with height. The sonic anemometers on OU2 demonstrate similar behavior but the features are less pronounced and the jump occurs at lower frequencies. The 2.5 m and 5 m levels of the ASU tower, which is near the east end of the canyon (see Figure 1), also have positive cosprectrum at low frequencies (see Figures 45 and 46). The 8.5 m ASU sonic (see Figure 47), on the other hand, exhibits predominantly negative cosprectrum.

Figures 48 and 49 show the spectra obtained from the LANL sonic anemometers placed on the northwest and southwest corners respectively of the building at the northeast corner of the canyon at z ~ 47.5 m. The flow on the northwest corner is predominantly southerly as prevailing flow hits the west side of the building and is deflected northward making the cross canyon component v the dominant component of the wind in this region. The along-canyon component u dominates the flow on the

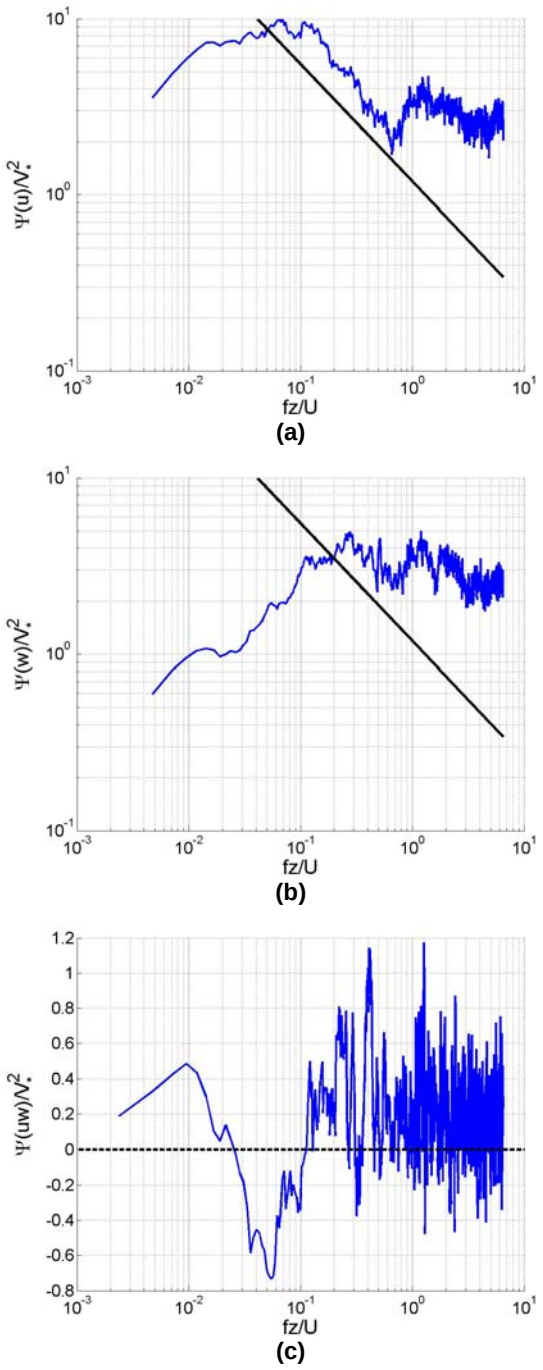

Figure 30. JU03 premultiplied spectra obtained from the UU sonic at z = 3.19 m. (a) along canyon PSD, (b) vertical PSD, and (c) along canyon-vertical cosprectrum. The black line in (a) and (b) is to indicate the $f^{-2/3}$ slope characteristic of the inertial subrange.

southwest corner of the building, but otherwise exhibits similar characteristics to those found on the northwest corner. These two sonic anemometers are not in close proximity to any small-scale sources of turbulence (with exception of boom on which they are mounted) and therefore only the large-scale building effects are evident in these regions. This is certainly not the case with the spectra shown in Figure 50, which are the spectra from the LANL sonic on the overhang of the building at the southeast of the canyon (see Figure 1). This sonic is located approximately 1 meter from the wall of the building as seen in the right side of Figure 4. Proximity to the wall has dramatically affected the spectra. The effects of the proximity to the wall are most evident in the cross-canyon component where the premultiplied PSD is constant (f^{-1} behavior non-premultiplied) for almost the entire range of frequencies measured. The cross-canyon eddies have been damped out due to the proximity to the wall affecting the energy transfer between flow scales.

Figure 51 shows the premultiplied along-canyon PSD for the LANL sonic on the southwest corner of the northeast building. This PSD was obtained using data from the time period of 0000 to 0300 CDT with a one-hour window in order to capture more of the low-frequency range. A 60-minute running-mean was used to calculate the fluctuating velocity components and the spectrum was smoothed using the same 11 data point running-mean. Hunt and Carlotti (2001) found through theoretical and numerical studies and Drobinski et al. (2004) found through field experiments that in the lower regions of the ASL the low frequency range of the premultiplied along-wind component PSD should be proportional to f (this trend is shown by the red line in the figure). They also found that the same premultiplied PSD should be constant over an intermediate range of frequencies and then exhibit inertial subrange behavior at high frequencies (the black line in the figure). It is interesting to note that these same behaviors are found in the roof-level sonic anemometers that are relatively free of local small-scale effects.

The two sonic anemometers at roof-level that are within the canyon were dominated by the along canyon component. The LANL sonic 5, which was located on the flagpole on top of the building at the southeast corner of the canyon had a significant cross-canyon component to the mean wind (see Figure 11). As discussed in Section 3.1, this sonic was located in the wake of the buildings immediately upstream. Figures 52 and 53 are respectively the spectra from the sonic on the flagpole before and after the flow has been rotated into the mean wind. The rotation flattens out the cross-wind component PSD since the portion of energy in the cross-canyon component due to the local mean wind has been transferred to the along- wind component giving the along-wind PSD a sharper peak.

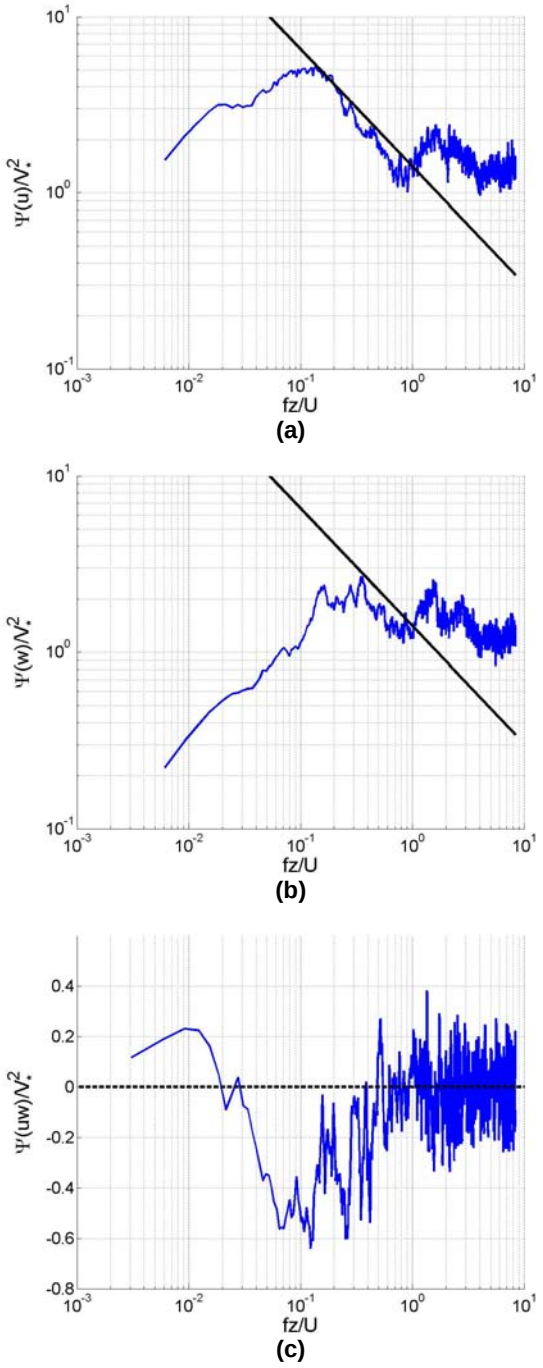

Figure 31. JU03 premultiplied spectra obtained from the UU sonic at z = 4.19 m. (a) along canyon PSD, (b) vertical PSD, and (c) along canyon-vertical cosprectrum. The black line in (a) and (b) is to indicate the $f^{-2/3}$ slope characteristic of the inertial subrange.

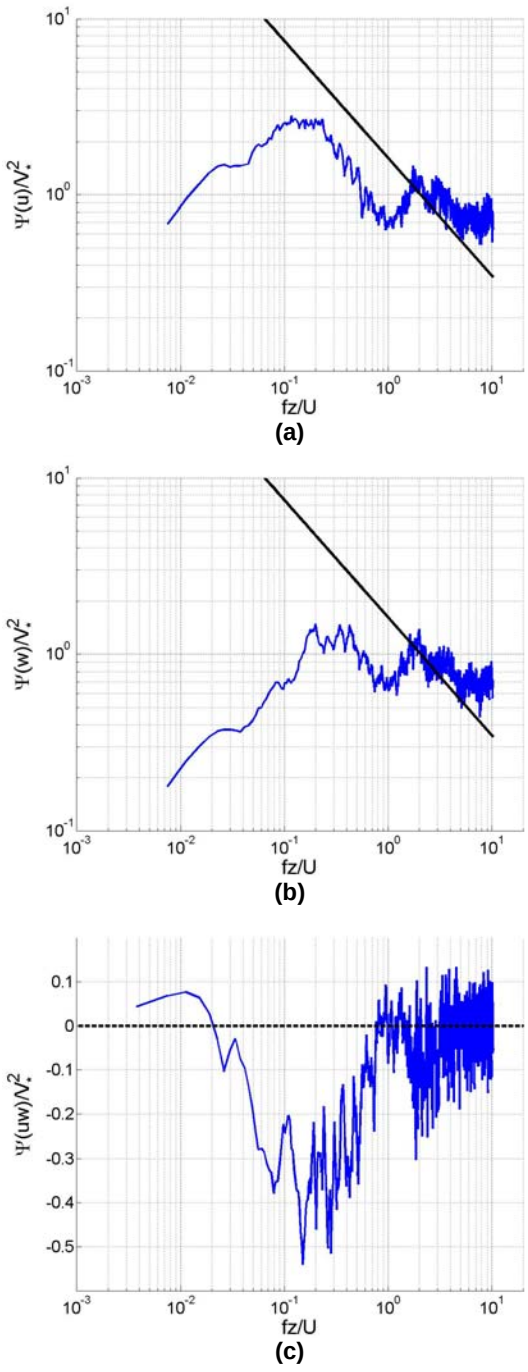

Figure 32. JU03 premultiplied spectra obtained from the UU sonic at z = 5.04 m. (a) along canyon PSD, (b) vertical PSD, and (c) along canyon-vertical cosprectrum. The black line in (a) and (b) is to indicate the $f^{-2/3}$ slope characteristic of the inertial subrange.

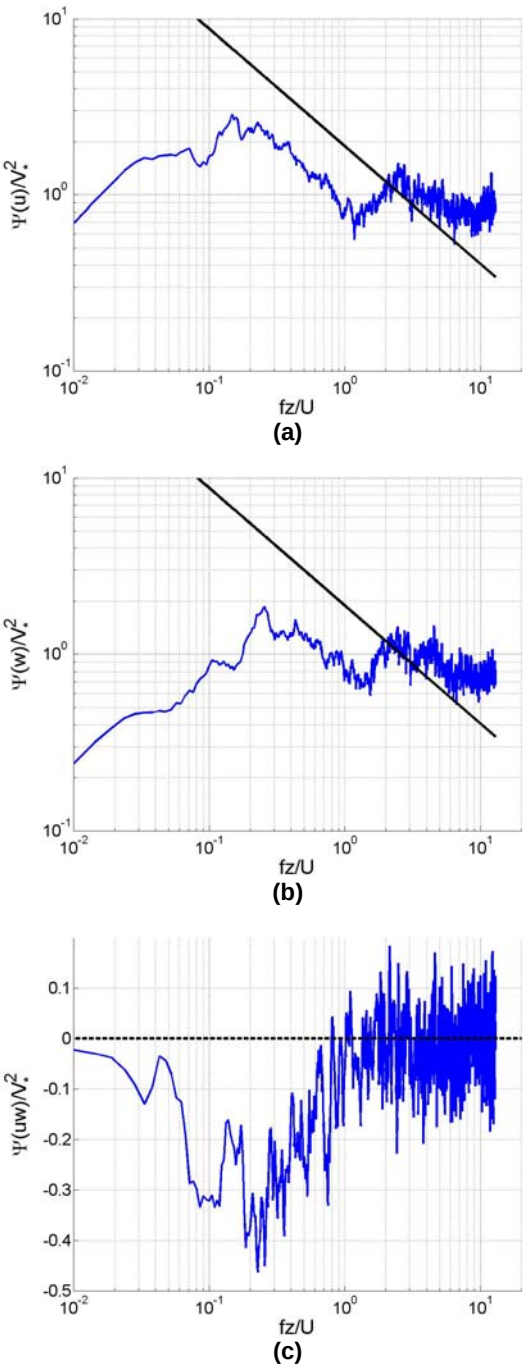

Figure 33. JU03 premultiplied spectra obtained from the UU sonic at z = 7.24 m. (a) along canyon PSD, (b) vertical PSD, and (c) along canyon-vertical cosprectrum. The black line in (a) and (b) is to indicate the $f^{-2/3}$ slope characteristic of the inertial subrange.

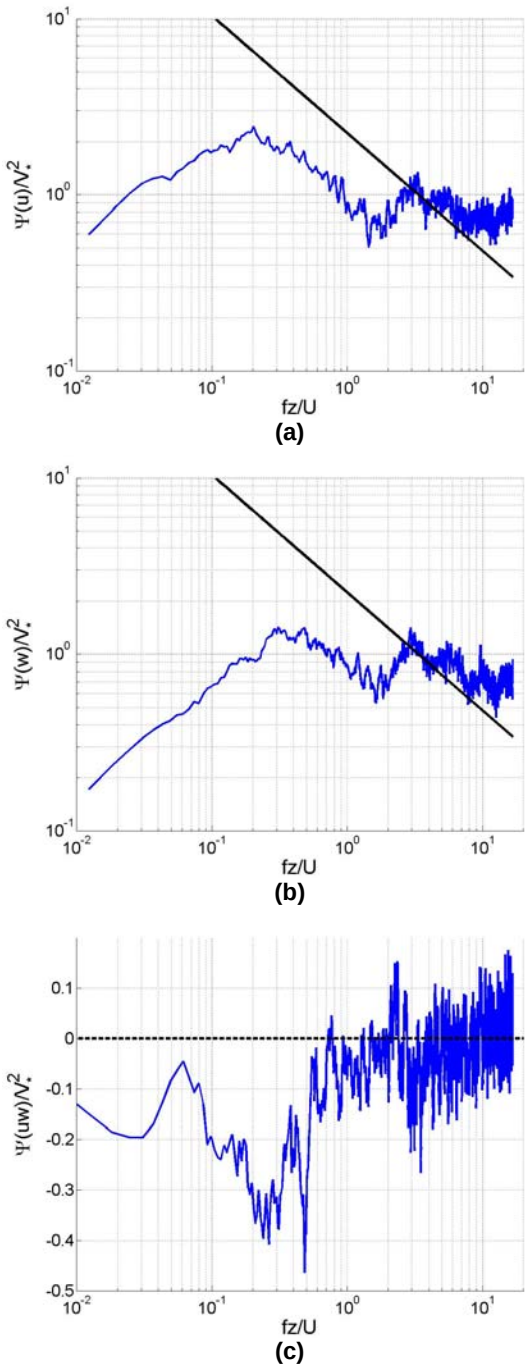

Figure 34. JU03 premultiplied spectra obtained from the UU sonic at z = 9.84 m. (a) along canyon PSD, (b) vertical PSD, and (c) along canyon-vertical cosprectrum. The black line in (a) and (b) is to indicate the $f^{-2/3}$ slope characteristic of the inertial subrange.

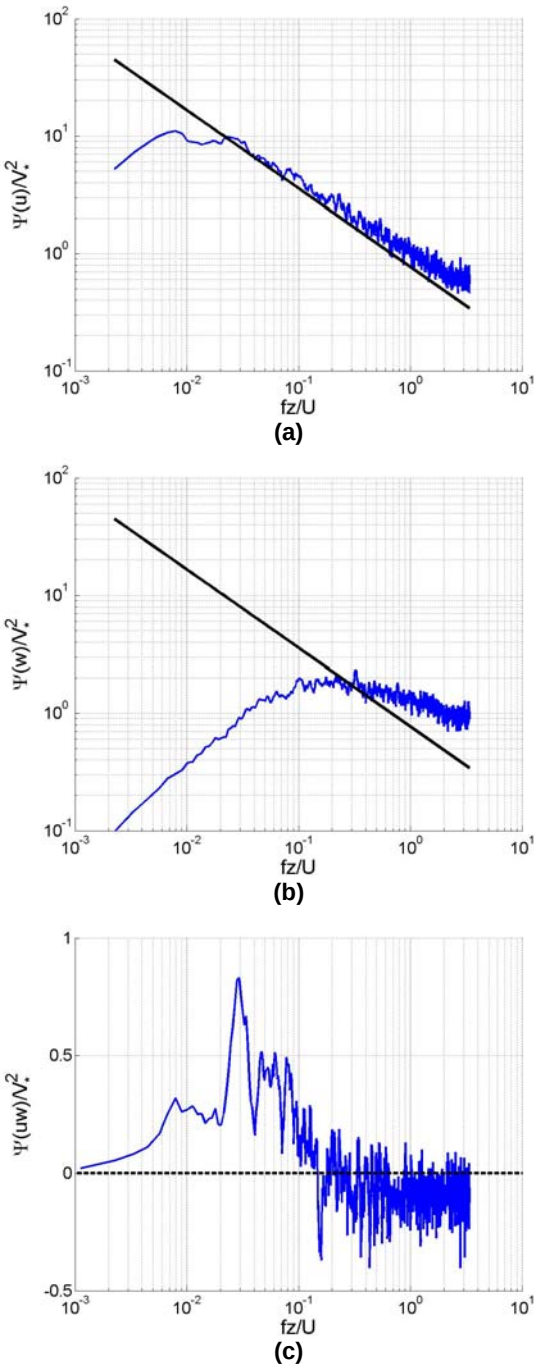

Figure 35. JU03 premultiplied spectra obtained from the OU1 sonic at z = 1.50 m. (a) along canyon PSD, (b) vertical PSD, and (c) along canyon-vertical cosprectrum. The black line in (a) and (b) is to indicate the $f^{-2/3}$ slope characteristic of the inertial subrange.

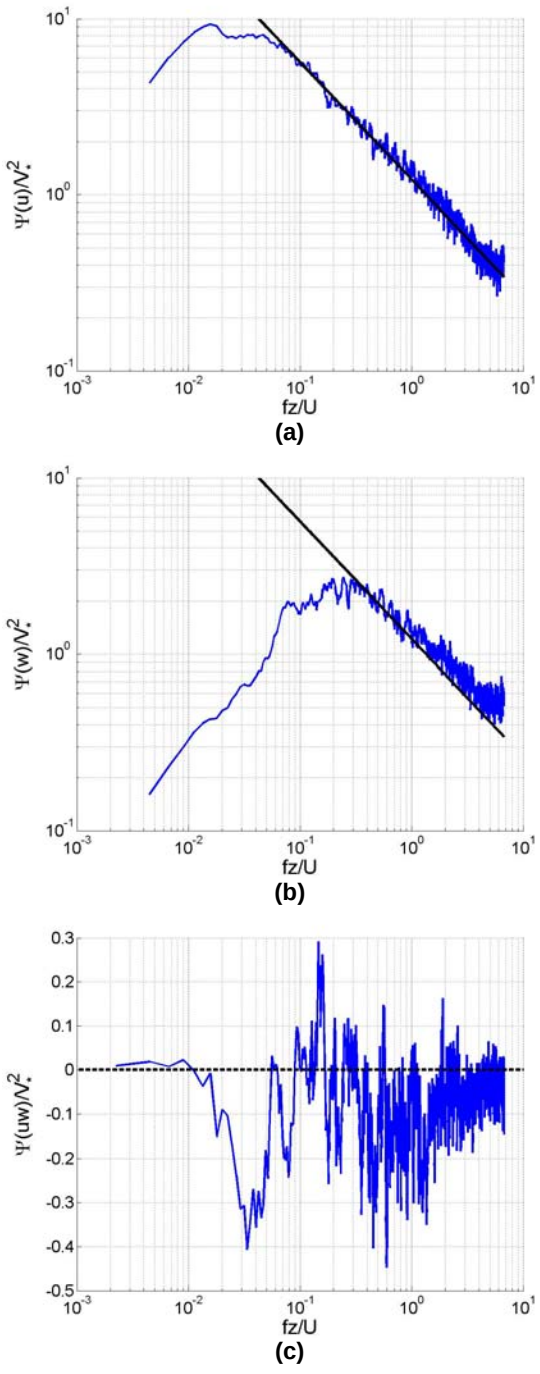

Figure 36. JU03 premultiplied spectra obtained from the OU1 sonic at z = 2.96 m. (a) along canyon PSD, (b) vertical PSD, and (c) along canyon-vertical cosprectrum. The black line in (a) and (b) is to indicate the $f^{-2/3}$ slope characteristic of the inertial subrange.

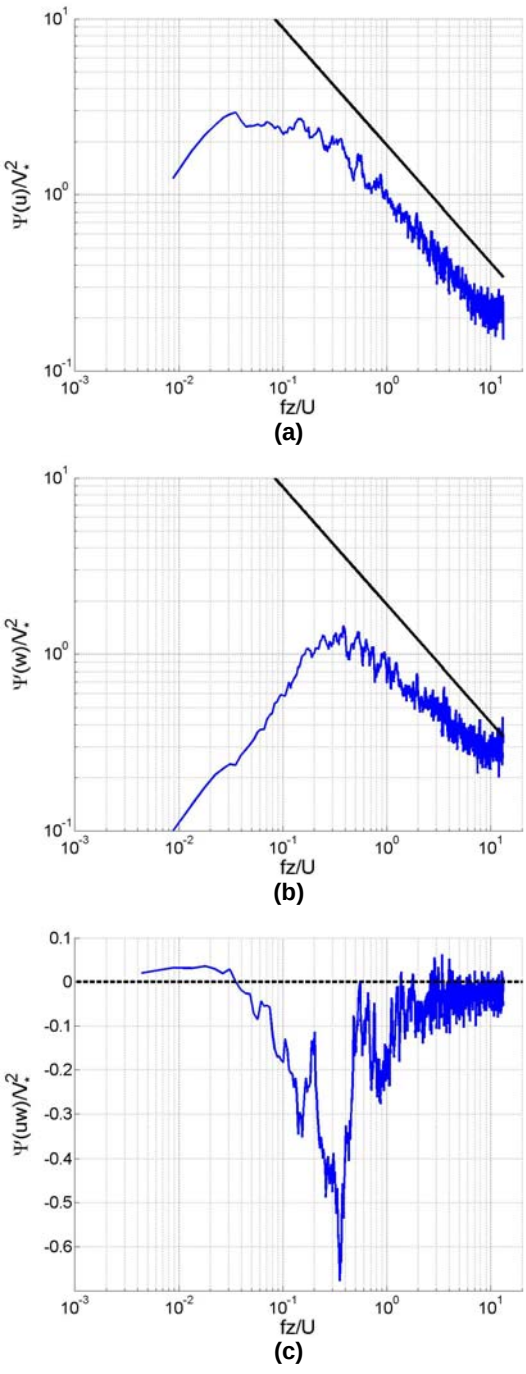

Figure 37. JU03 premultiplied spectra obtained from the OU1 sonic at z = 5.97 m. (a) along canyon PSD, (b) vertical PSD, and (c) along canyon-vertical cosprectrum. The black line in (a) and (b) is to indicate the $f^{-2/3}$ slope characteristic of the inertial subrange.

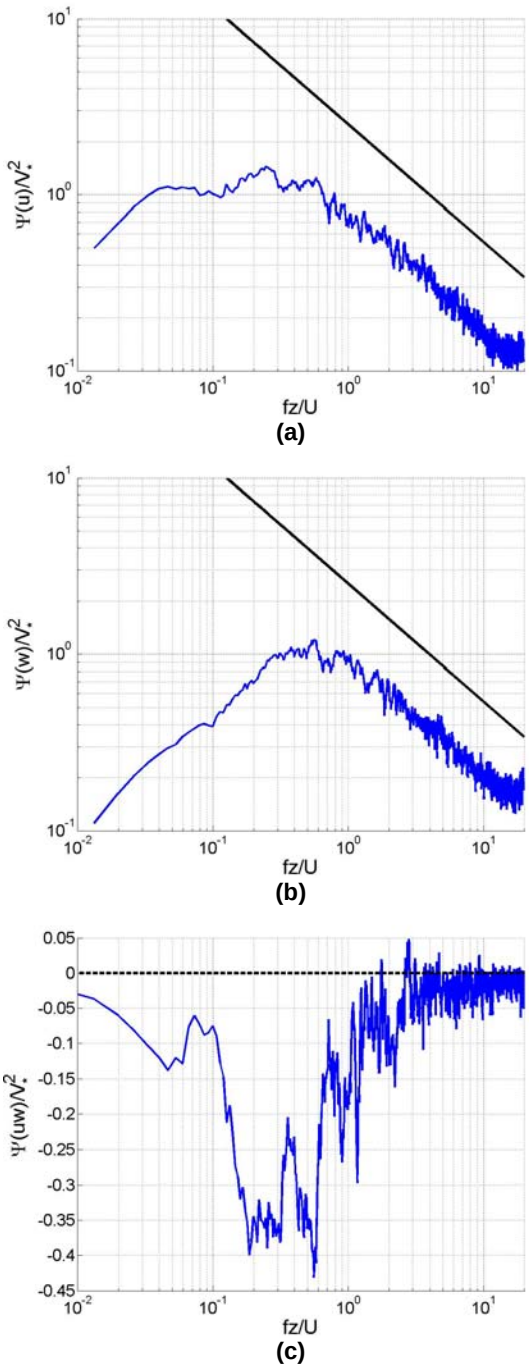

Figure 38. JU03 premultiplied spectra obtained from the OU1 sonic at z = 9.91 m. (a) along canyon PSD, (b) vertical PSD, and (c) along canyon-vertical cosprectrum. The black line in (a) and (b) is to indicate the $f^{-2/3}$ slope characteristic of the inertial subrange.

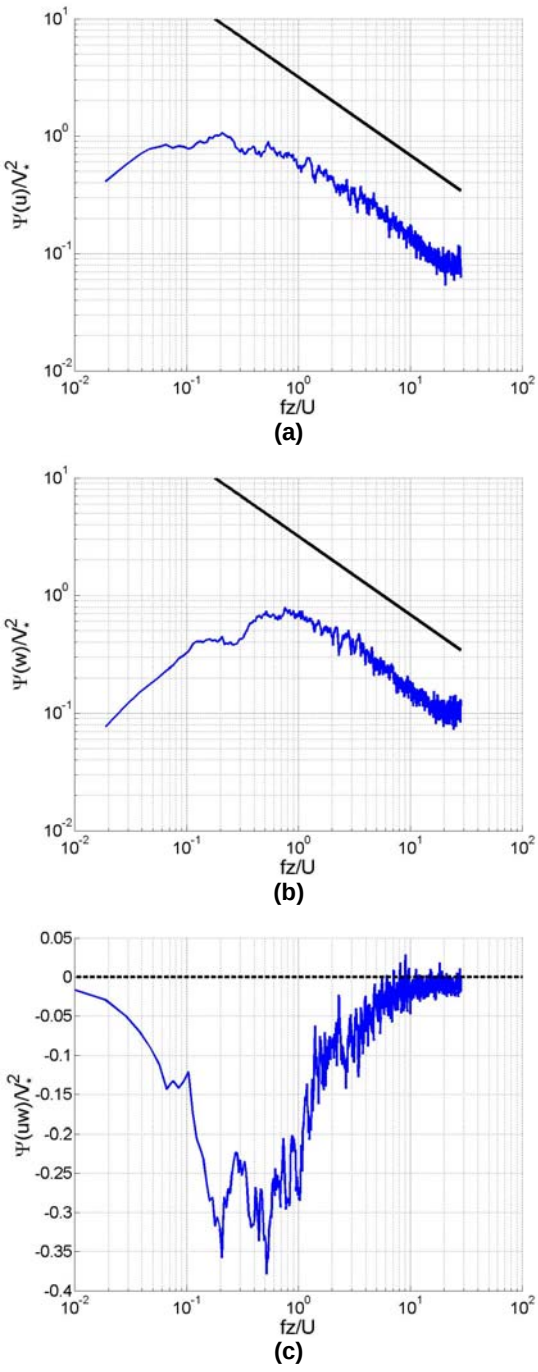

Figure 39. JU03 premultiplied spectra obtained from the OU1 sonic at z = 15.08 m. (a) along canyon PSD, (b) vertical PSD, and (c) along canyon-vertical cosprectrum. The black line in (a) and (b) is to indicate the $f^{-2/3}$ slope characteristic of the inertial subrange.

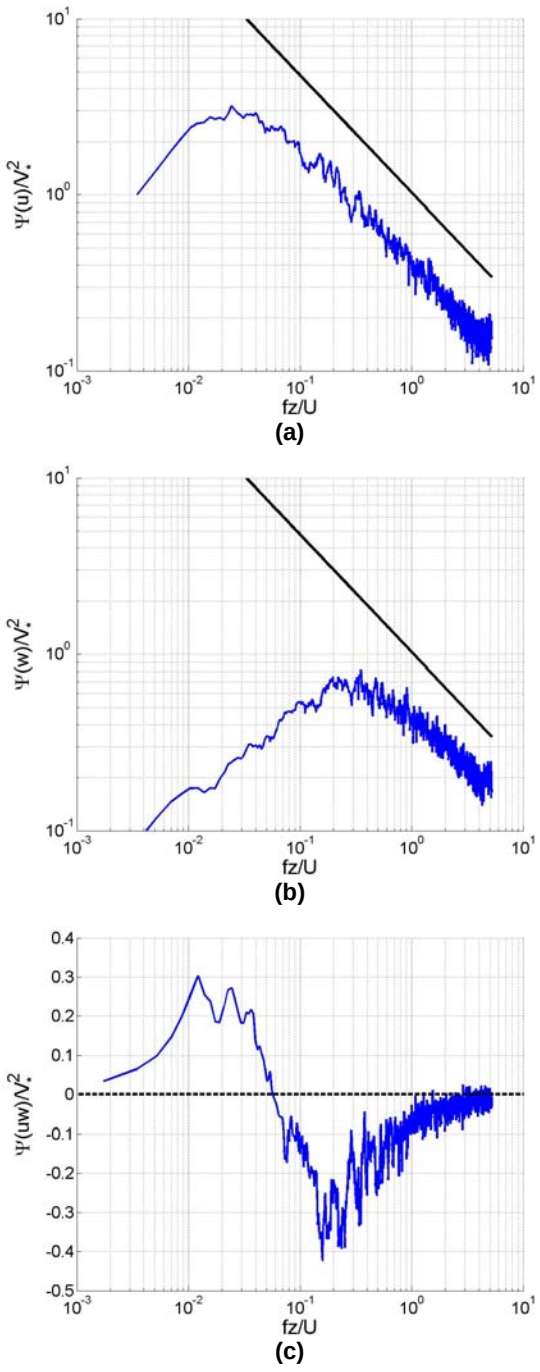

Figure 40. JU03 premultiplied spectra obtained from OU2 sonic at z = 1.5 m. (a) along canyon PSD, (b) vertical PSD, and (c) along canyon-vertical cosprectrum. The black line in (a) and (b) is to indicate the $f^{-2/3}$ slope characteristic of the inertial subrange.

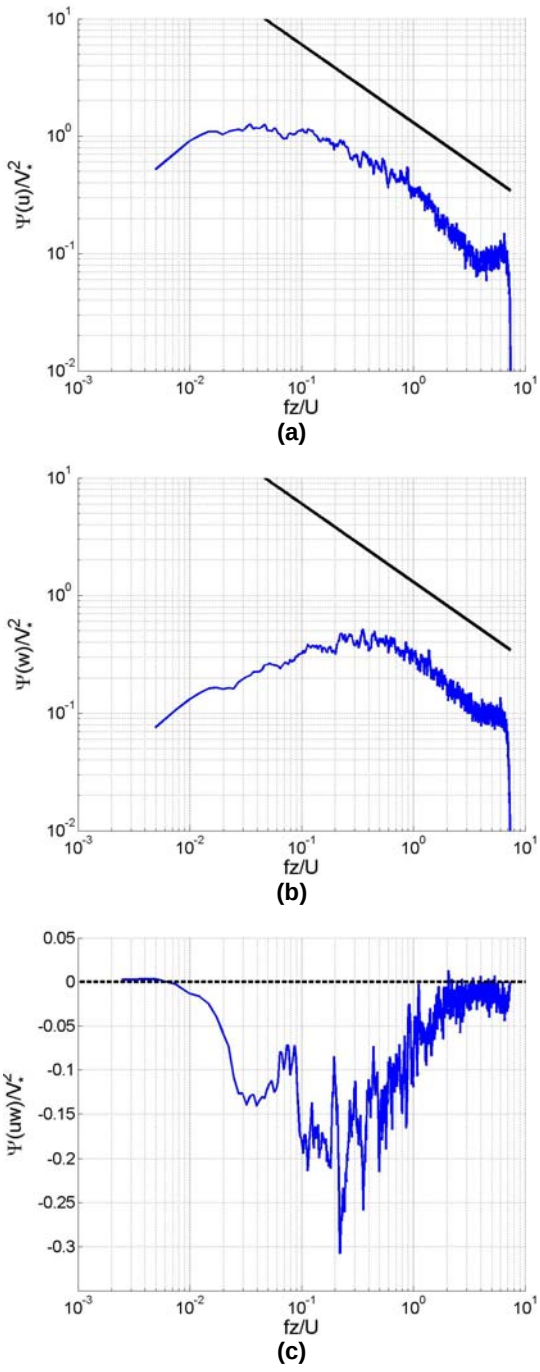

Figure 41. JU03 premultiplied spectra obtained from OU2 sonic at z = 3.00 m. (a) along canyon PSD, (b) vertical PSD, and (c) along canyon-vertical cosprectrum. The black line in (a) and (b) is to indicate the $f^{-2/3}$ slope characteristic of the inertial subrange.

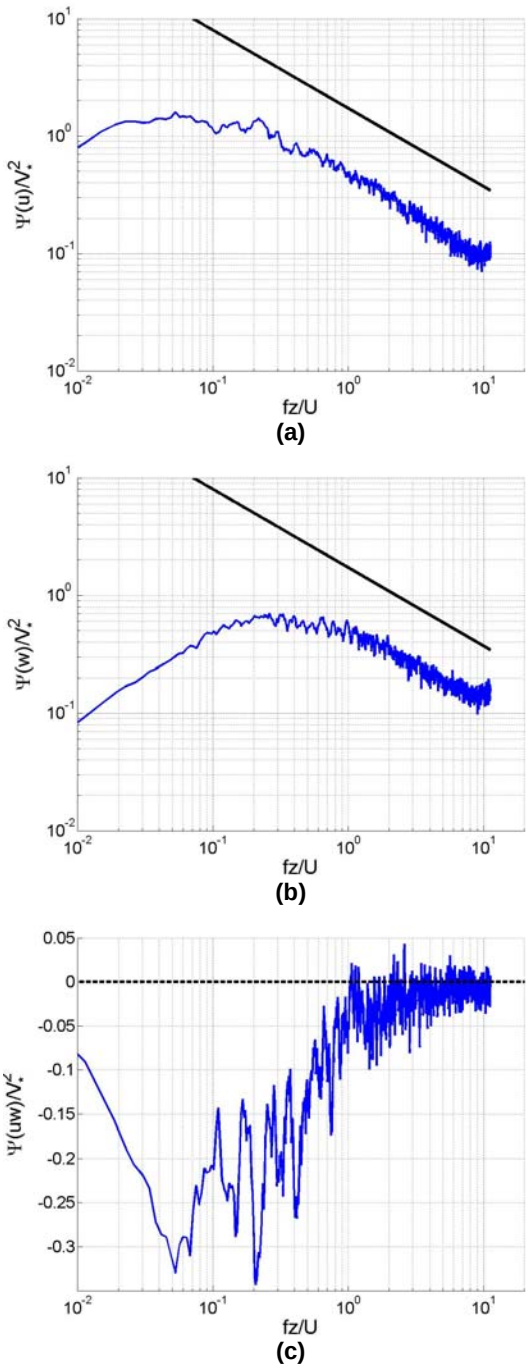

Figure 42. JU03 premultiplied spectra obtained from OU2 sonic at z = 5.46 m. (a) along canyon PSD, (b) vertical PSD, and (c) along canyon-vertical cosprectrum. The black line in (a) and (b) is to indicate the $f^{-2/3}$ slope characteristic of the inertial subrange.

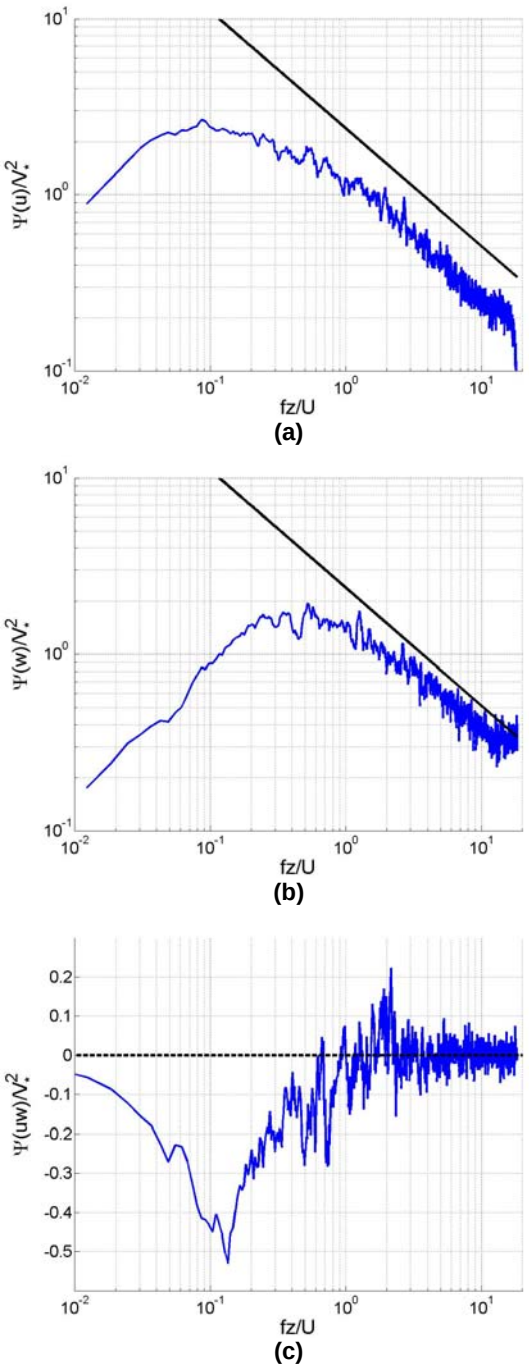

Figure 43. JU03 premultiplied spectra obtained from OU2 sonic at z = 9.86 m. (a) along canyon PSD, (b) vertical PSD, and (c) along canyon-vertical cosprectrum. The black line in (a) and (b) is to indicate the $f^{-2/3}$ slope characteristic of the inertial subrange.

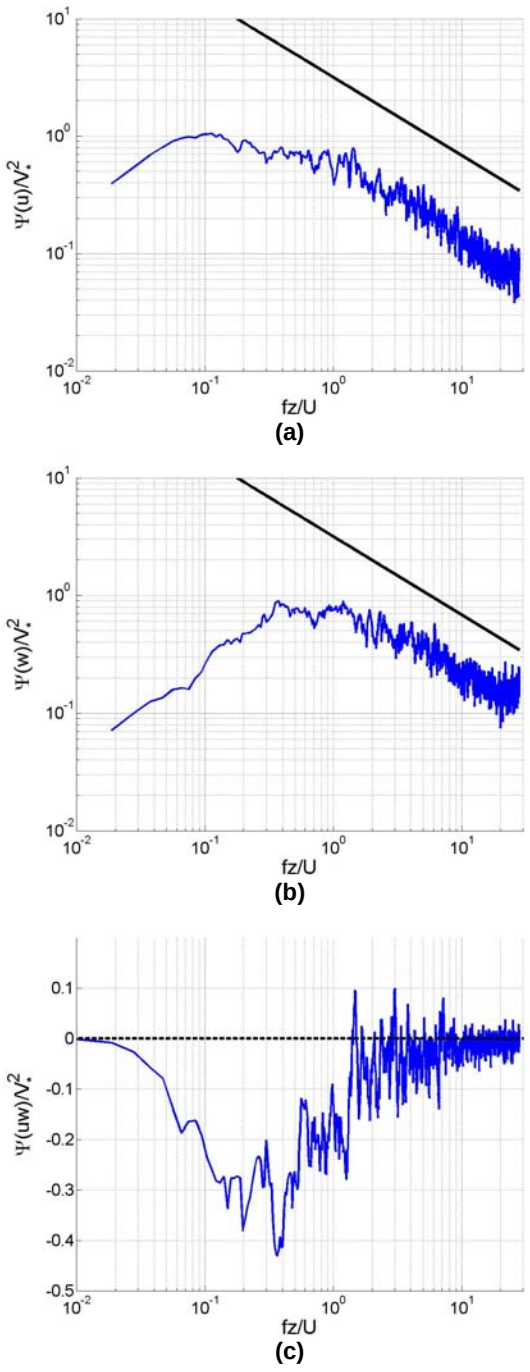

Figure 44. JU03 premultiplied spectra obtained from OU2 sonic at z = 15.65 m. (a) along canyon PSD, (b) vertical PSD, and (c) along canyon-vertical cosprectrum. The black line in (a) and (b) is to indicate the $f^{-2/3}$ slope characteristic of the inertial subrange.

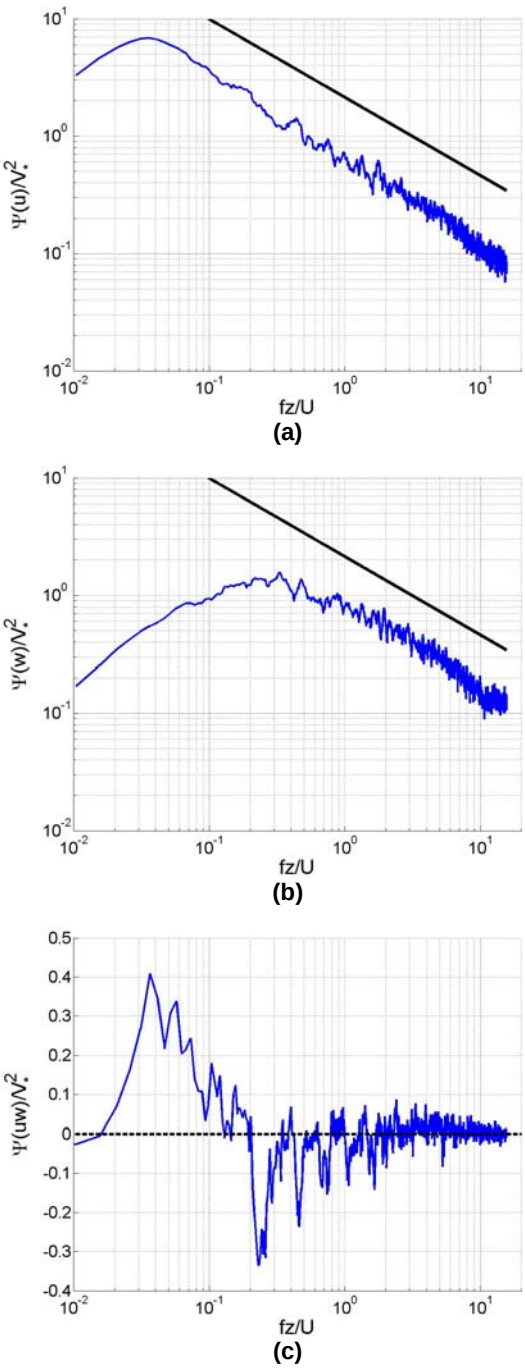

Figure 45. JU03 premultiplied spectra obtained from the ASU sonic at z = 2.5 m. (a) along canyon PSD, (b) vertical PSD, and (c) along canyon-vertical cosprectrum. The black line in (a) and (b) is to indicate the $f^{-2/3}$ slope characteristic of the inertial subrange.

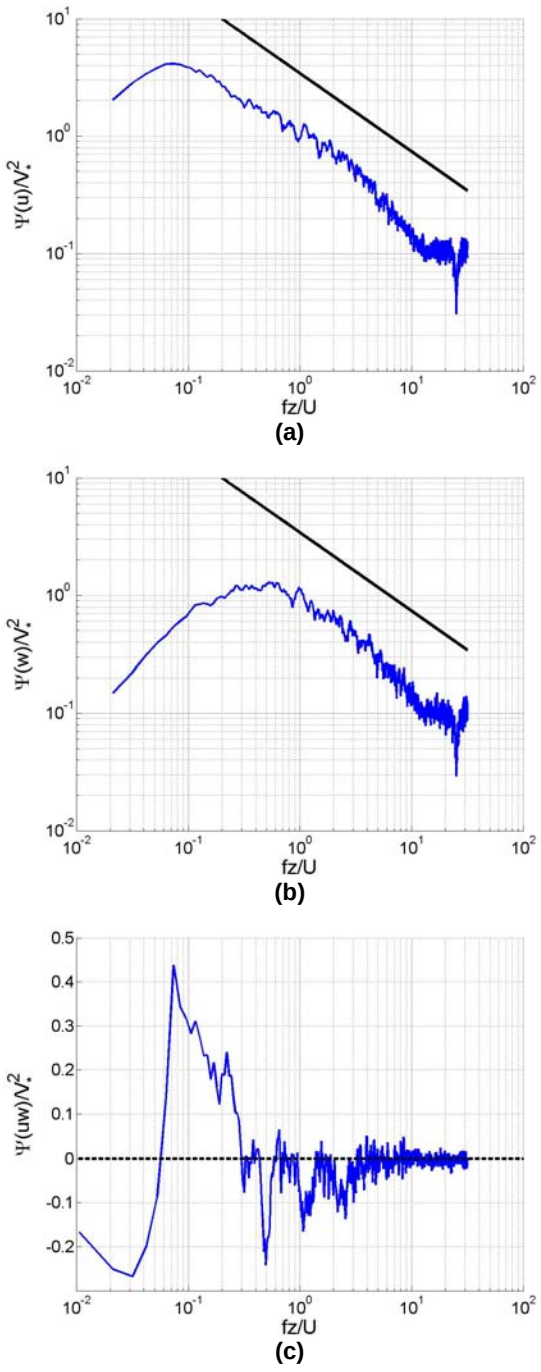

Figure 46. JU03 premultiplied spectra obtained from the ASU sonic at z = 5.0 m. (a) along canyon PSD, (b) vertical PSD, and (c) along canyon-vertical cosprectrum. The black line in (a) and (b) is to indicate the $f^{-2/3}$ slope characteristic of the inertial subrange.

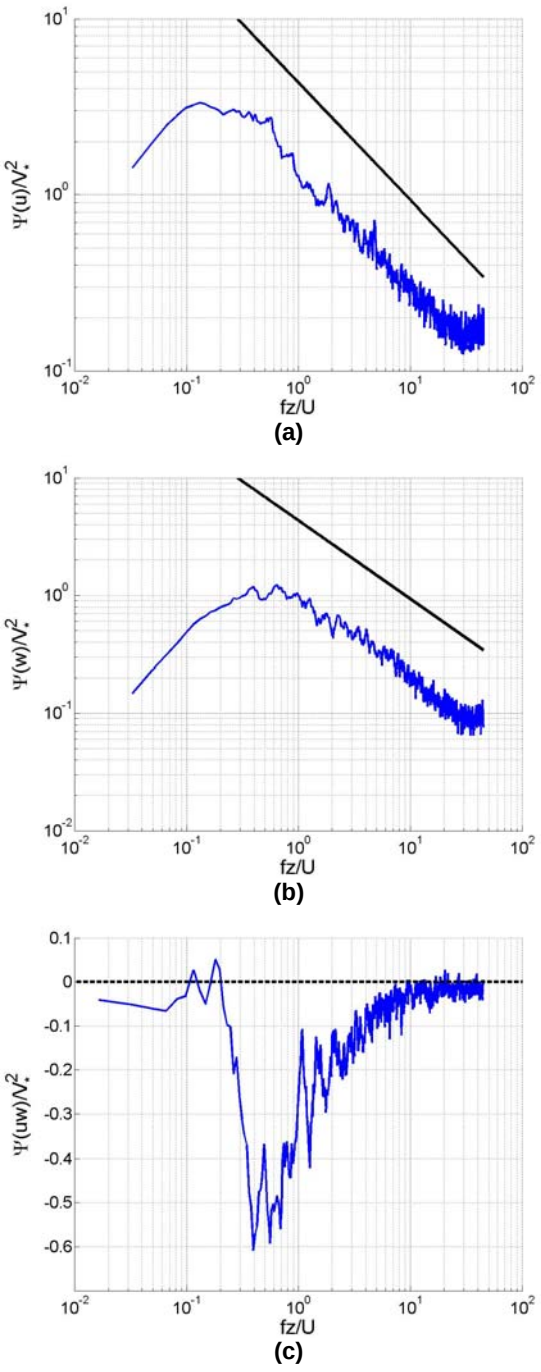

Figure 47. JU03 premultiplied spectra obtained from the ASU sonic at z = 8.5 m. (a) along canyon PSD, (b) vertical PSD, and (c) along canyon-vertical cosprectrum. The black line in (a) and (b) is to indicate the $f^{-2/3}$ slope characteristic of the inertial subrange.

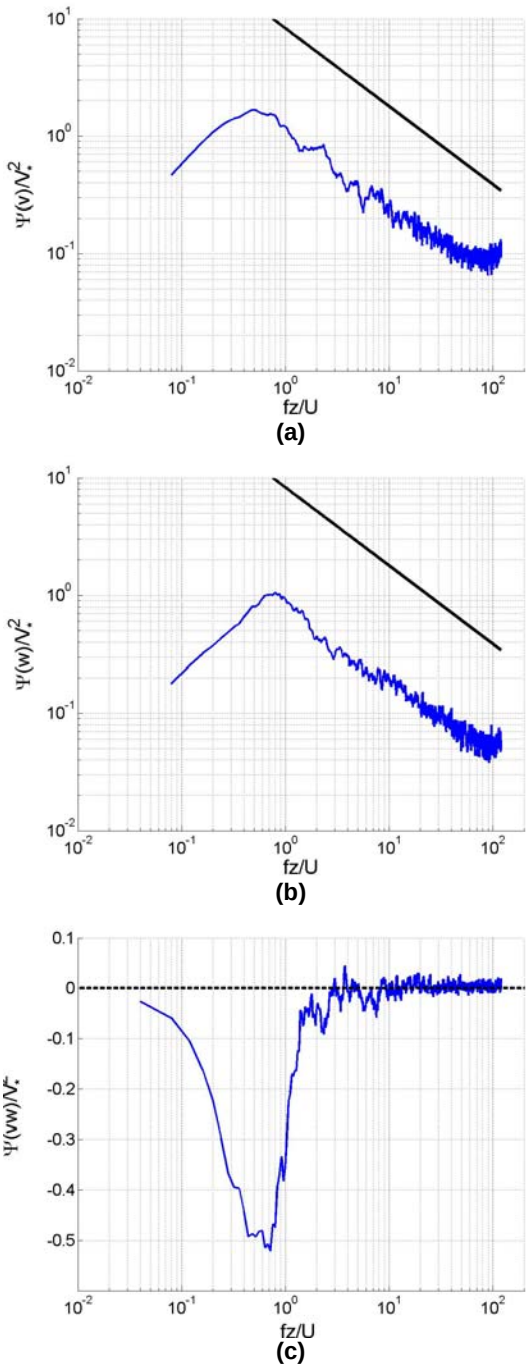

Figure 48. JU03 premultiplied spectra obtained from the LANL sonic at z ~ 47.5 m on the northwest corner of the building at the northeast corner of the Park Avenue canyon. (a) cross canyon PSD, (b) vertical PSD, and (c) cross canyon-vertical cosprectrum. The black line in (a) and (b) is to indicate the $f^{-2/3}$ slope characteristic of the inertial subrange.

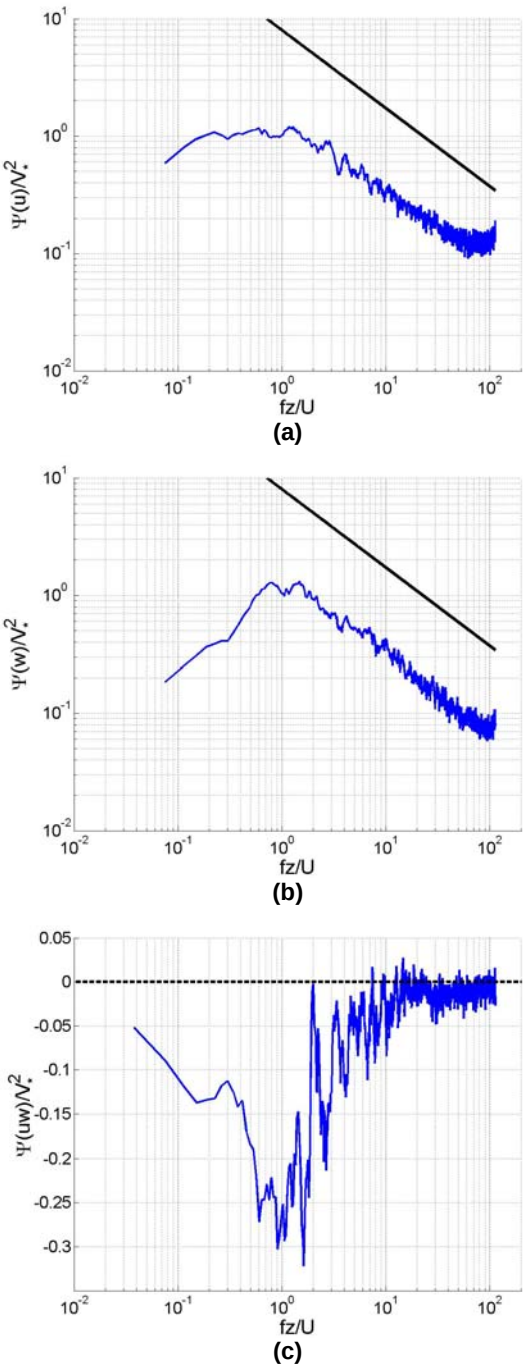

Figure 49. JU03 premultiplied spectra obtained from the LANL sonic at z ~ 47.5 m on the southwest corner of the building at the northeast corner of the Park Avenue canyon. (a) along canyon PSD, (b) vertical PSD, and (c) along canyon-vertical cosprectrum. The black line in (a) and (b) is to indicate the $f^{-2/3}$ slope characteristic of the inertial subrange.

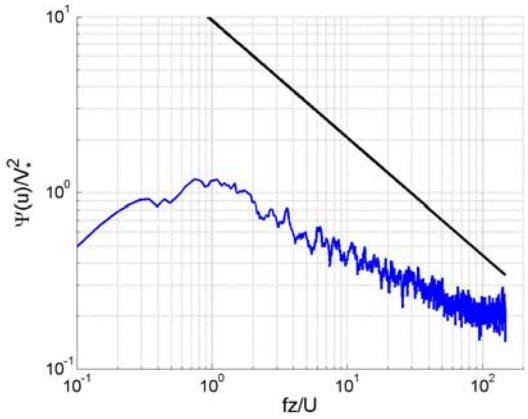

(a)

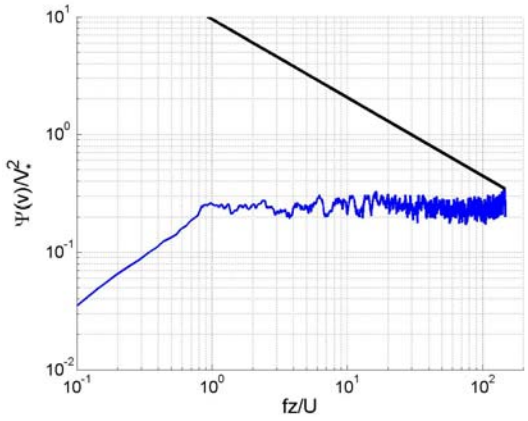

(b)

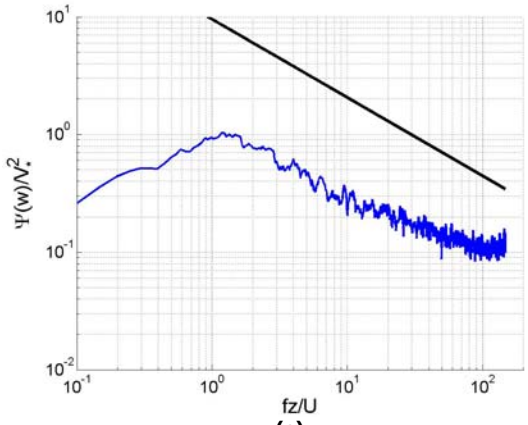

(c)

Figure 50. JU03 premultiplied spectra obtained from the LANL sonic at z ~ 45.3 m hanging over the side of the building at the southeast corner of the Park Avenue canyon. (a) along-canyon PSD, (b) cross-canyon PSD, and (c) vertical PSD. The black line is to indicate the $f^{-2/3}$ slope characteristic of the inertial subrange.

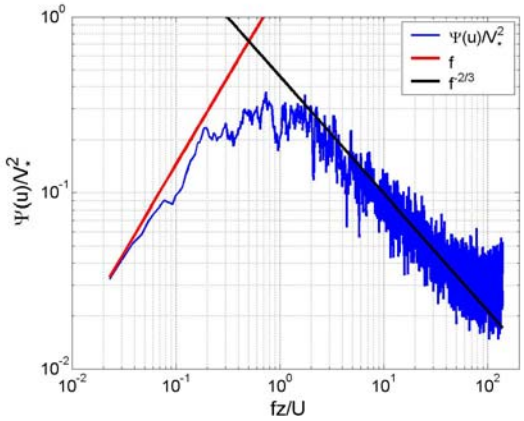

Figure 51. JU03 premultiplied PSD of along-canyon winds taken from the LANL sonic on the southwest corner of the northeast building in the canyon. Spectra shown is taken from 05:00 to 08:00 UTC with 1 hour averaging windows.

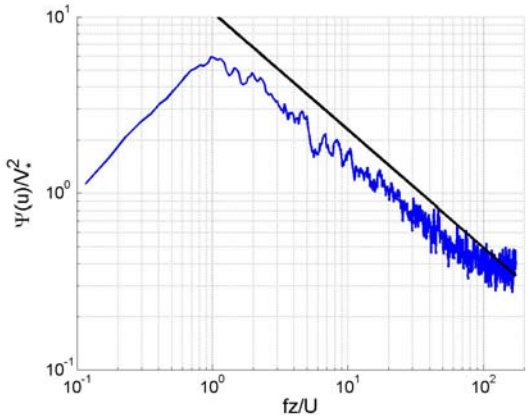

(a)

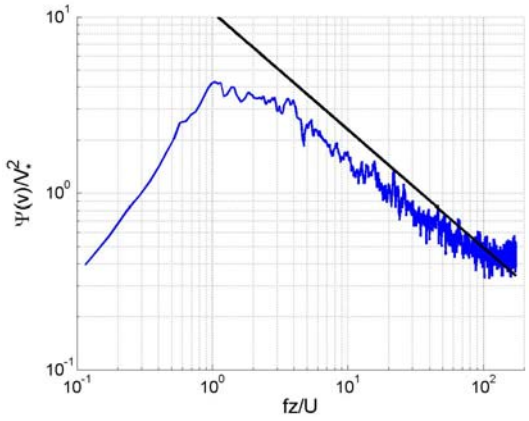

(b)

Figure 52. JU03 premultiplied spectra obtained from the LANL sonic at z ~ 47.7 m on the flagpole of the building at the southeast corner of the Park Avenue canyon. (a) along canyon PSD, (b) cross canyon PSD. The black line is to indicate the $f^{-2/3}$ slope characteristic of the inertial subrange.

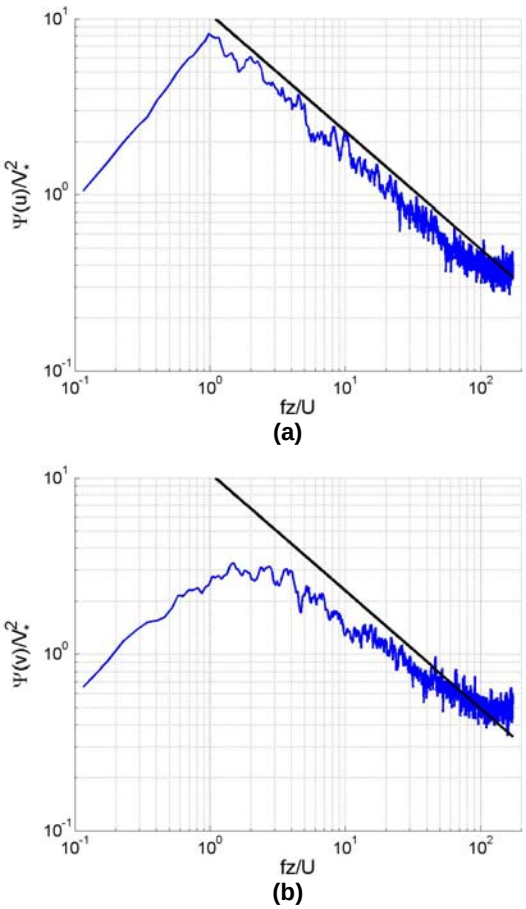

Figure 53. JU03 premultiplied spectra using winds rotated into the mean wind obtained from the LANL sonic at z ~ 47.7 m on the flagpole of the building at the southeast corner of the Park Avenue canyon. (a) along-wind PSD, (b) cross-wind PSD. The black line is to indicate the $f^{-2/3}$ slope characteristic of the inertial subrange.

3.4 *MUST Spectra*

In order to produce the spectra from MUST the fluctuating components of the wind were determined using a 15-minute linear detrending scheme. As such u is the component of the wind vector aligned with the mean wind direction, v is the crosswind component, and w is the vertical component. Since the obstacle imposed flow scales are smaller in MUST than in JU03 a 5-minute window was used in most cases to produce the spectra and the resulting spectra have been smoothed using an 11 data point running-mean.

Due to the fact that all of the structures in MUST were the same size and arranged in a regular array, regular flow features develop throughout the array which are evident in the spectra. The vortex shedding adds energy over a short band of frequencies in the PSD and cosprectrum. Contrast this behavior with the spectra from JU03 data where the complex morphology causes energy to be added over a broad range of frequencies. This effect is seen at all levels of the UU tower but is most striking at the 3.7 m level, which is in the RSL of the array. Figure 54 is the premultiplied PSD of the along-wind component of velocity taken at the 3.7 m level of the UU tower plotted on a semi-log scale to accentuate some of the features of the PSD. A 10-minute window was used in order to capture more of the low frequency range. Note the plateau in the spectrum before the large jump in the spectrum that occurs between fz/U = 0.1 and 0.2. This plateau is present in undisturbed ASL as discussed in reference to Figure 51. The vortex shedding on the regular array of obstacles has added energy over a discrete range of frequencies producing the jump in PSD.

Figures 55-59 are premultiplied spectra from the UU tower in the southern-most canyon of the MUST array (see Figures 7 and 8) at heights 0.56 m, 1.0 m, 1.8 m, 2.6 m, and 3.7 m respectively. The vertical PSD transition from a rounded peak in the lower levels of the canyon to a sharp peak in the upper levels of the canyon and into the RSL, while the opposite is true of the along-wind PSD. These two phenomena are likely the result of the energy containing eddies in the RSL, whether they are a result of the background ASL turbulence or vortex shedding off of the obstacles in the array, entering the canyon. In the RSL the eddies are not as restricted by geometry. When these larger-scale eddies enter the canyon and the canyon geometry and proximity to the ground affect the flow scales. As was found in the JU03 spectra the along-wind PSD peaks at much lower frequencies than does the vertical PSD. Thus the large-scale horizontal eddies from the ASL turbulence are damped out by the restriction of the canyon width, while the intermediate flow scales are relatively unaffected. The smaller-scale vertical motions are distorted as these motions encounter the earth's surface. Another result of the difference in flow scales at which the PSD peak is that the cospectra tend to peak at a flow scale between the peaks in the PSD. A pronounced peak is seen in

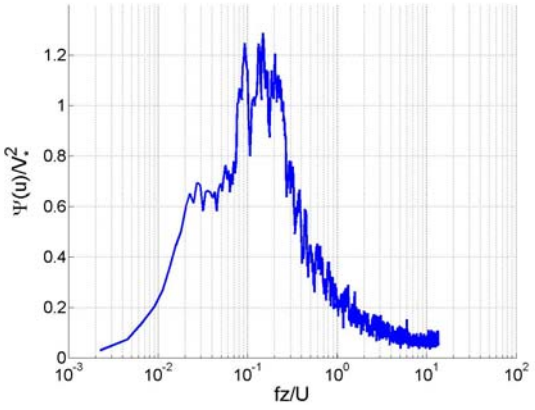

Figure 54. MUST along-wind PSD from the UU sonic at z = 3.7 m using a 10-minute window. Note the plateau in the spectra before the region where vortex shedding adds energy to the flow (fz/U = 0.1 to 0.2).

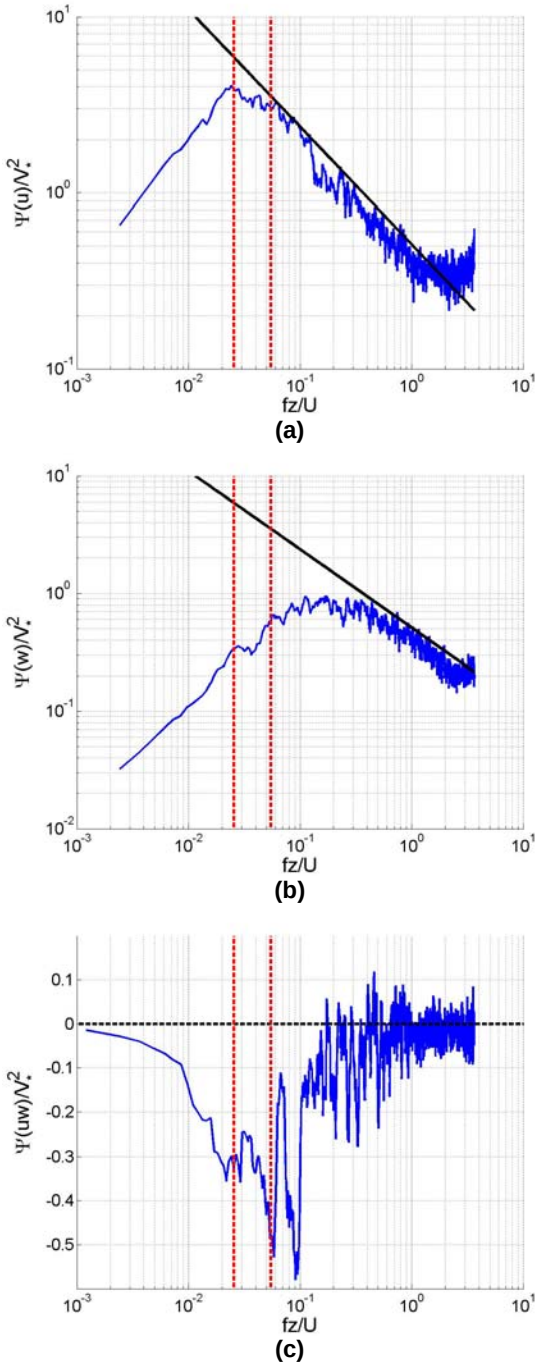

Figure 55. MUST premultiplied spectra obtained from the UU sonic at z = 0.56 m. (a) along wind PSD, (b) vertical PSD, and (c) along wind-vertical cosprectrum. The black line in (a) and (b) is to indicate the $f^{-2/3}$ slope characteristic of the inertial subrange. The vertical dashed red lines indicate the range of frequencies corresponding to vortex shedding found in Figure 54.

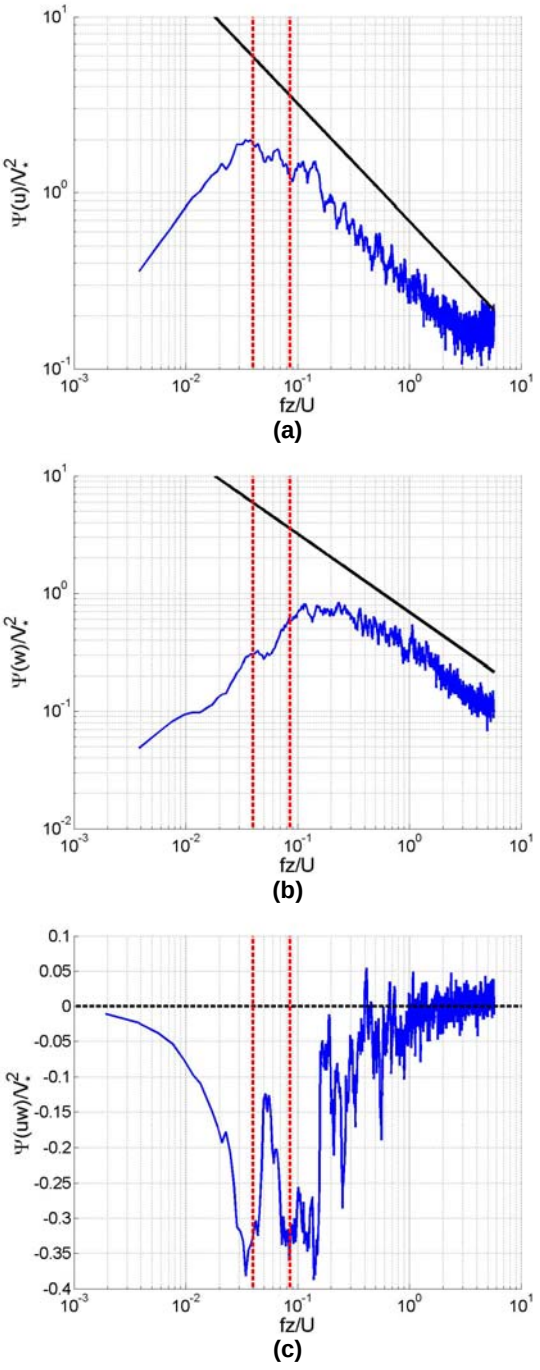

Figure 56. MUST premultiplied spectra obtained from the UU sonic at z = 1.0 m. (a) along wind PSD, (b) vertical PSD, and (c) along wind-vertical cosprectrum. The black line in (a) and (b) is to indicate the $f^{-2/3}$ slope characteristic of the inertial subrange. The vertical dashed red lines indicate the range of frequencies corresponding to vortex shedding found in Figure 54.

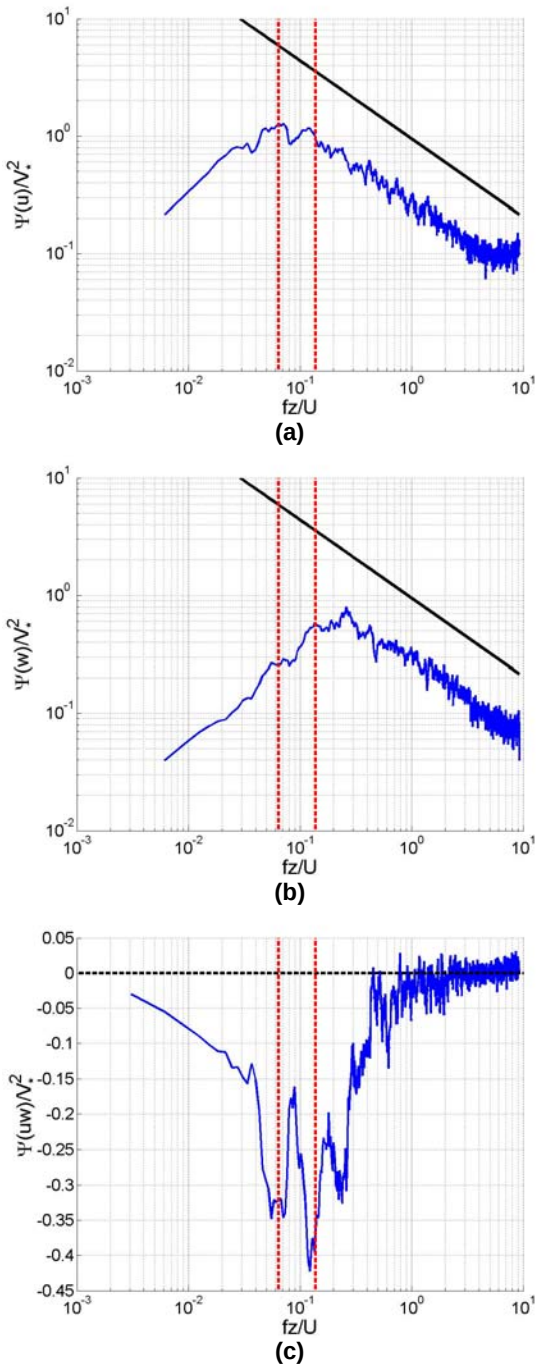

Figure 57. MUST premultiplied spectra obtained from the UU sonic at z = 1.8 m. (a) along wind PSD, (b) vertical PSD, and (c) along wind-vertical cosprectrum. The black line in (a) and (b) is to indicate the $f^{-2/3}$ slope characteristic of the inertial subrange. The vertical dashed red lines indicate the range of frequencies corresponding to vortex shedding found in Figure 54.

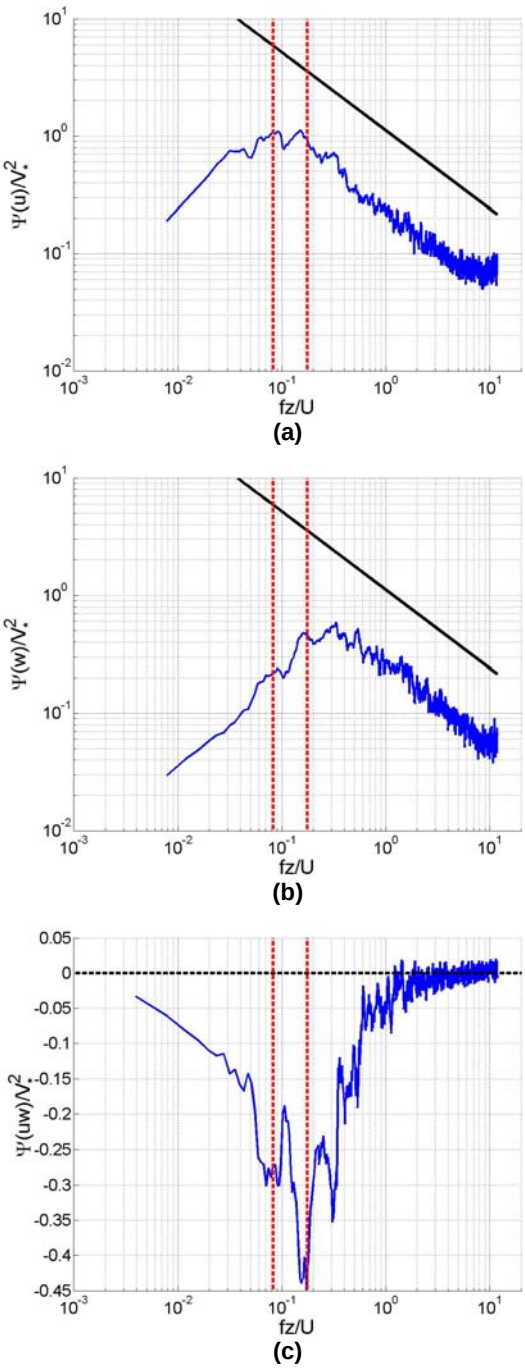

Figure 58. MUST premultiplied spectra obtained from the UU sonic at z = 2.6 m. (a) along wind PSD, (b) vertical PSD, and (c) along wind-vertical cosprectrum. The black line in (a) and (b) is to indicate the $f^{-2/3}$ slope characteristic of the inertial subrange. The vertical dashed red lines indicate the range of frequencies corresponding to vortex shedding found in Figure 54.

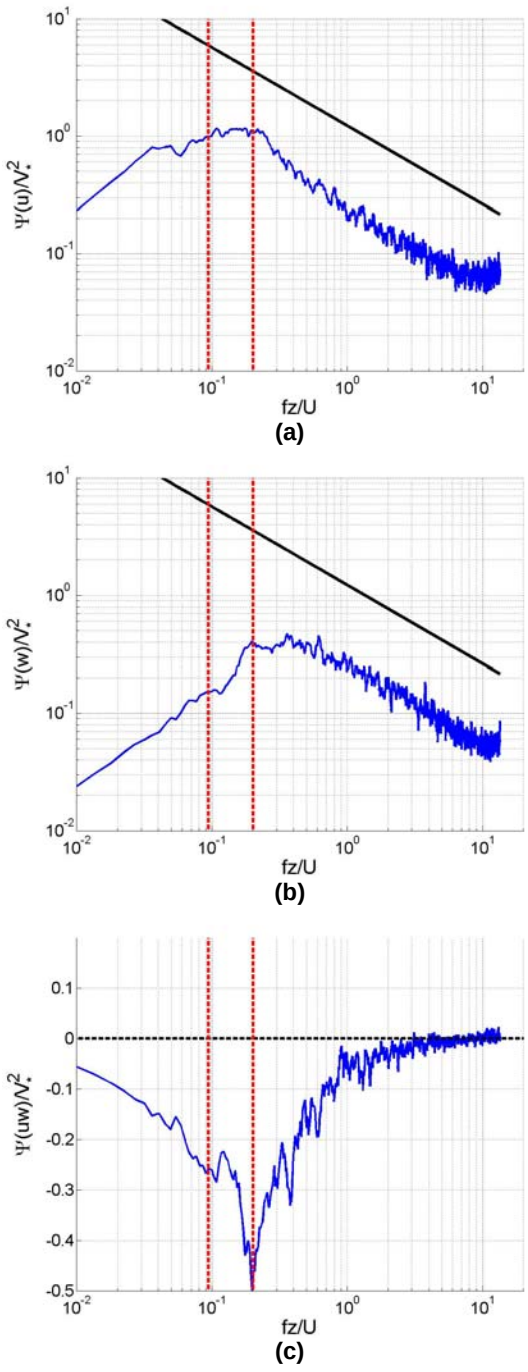

Figure 59. MUST premultiplied spectra obtained from the UU sonic at z = 3.7 m. (a) along wind PSD, (b) vertical PSD, and (c) along wind-vertical cosprectrum. The black line in (a) and (b) is to indicate the $f^{-2/3}$ slope characteristic of the inertial subrange. The vertical dashed red lines indicate the range of frequencies corresponding to vortex shedding found in Figure 54.

each of the along-wind to vertical cospectrum, which generally corresponds to the upper limit of the vortex shedding frequency range found in Figure 54, with exception of the two lowest sonic anemometers on the UU tower which peak at slightly higher frequencies. Thus the vortex shedding plays a major role in the vertical transport within the array. The peak in the cospectrum is well defined in the RSL and becomes progressively less defined with increasing distance below building height.

Figures 60-62 are the spectra obtained from the LANL sonic anemometers located above and in the wake of container L4 at z = 3.8 m, 2.37 m, and 1.7 m respectively (see Figure 8). Care must be taken in the interpretation of these spectra for two reasons: first, the LANL sonic anemometers were found to have inconsistent sampling frequencies due to a hardware conflict; and second, the sonic anemometers from the LANL tower were not in the same horizontal position. While the two RSL sonic anemometers have very similar characteristics (see Figures 59 and 60), the differences in the spectra demonstrate some of the inhomogeneous nature of the RSL. The cospectrum measured in the RSL by the UU tower has a sharper peak, while that of the LANL tower has a broader peak. The along-wind PSD measured by the UU sonic anemometer has a large f^{-1} (if plotted non-premultiplied) at the peak than does the LANL sonic. The opposite is true of the vertical PSD. The LANL sonic is closer to an obstacle than is the UU sonic. One would expect the vortices shed off of the obstacles in the array to have different structures just above the downwind edge of the obstacle than in the middle of the gap in between obstacles.

The individual obstacle effects are even more evident in spectra taken near H (see Figures 58 and 61). The LANL sonic is much closer to an obstacle than is the UU sonic at a similar height, thus the obstacle effects are much more prevalent in the spectra from the LANL sonic. A broad peak in the along-wind and cross-wind component PSD occur at higher frequencies than are found on the other sonic anemometers which is followed by a large f^{-1} region in the intermediate scales. The behavior is reminiscent of the behavior found in the cross-canyon component PSD from LANL sonic 2 from JU03 (see Figure 50). The fact that the behavior is found in both horizontal components is due to the fact that the flow was not aligned with the obstacle, unlike the flow in the urban canyon of JU03. The high frequency limit of this behavior also coincides with an abrupt change in behavior in the PSD for all components. This transition frequency roughly corresponds to a length scale of 0.8 m, which is close to distance of this sonic from the obstacle wall. After this transition frequency the horizontal PSD begin exhibiting trends typical of the inertial subrange, while the vertical PSD, which briefly followed inertial subrange trends at narrow band of frequencies lower than the transition frequency, ceases to follow the same trends at higher frequencies.

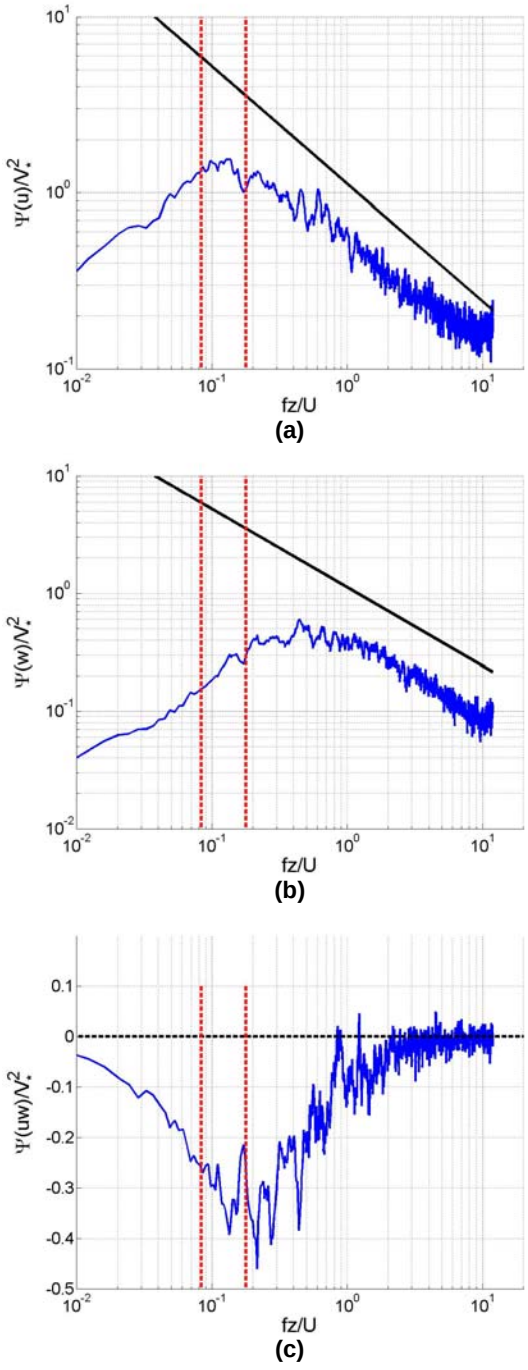

Figure 60. MUST premultiplied spectra obtained from the LANL sonic at z = 3.8 m, located above the trailing edge of the container on the south side of the simulated urban canyon. (a) along wind PSD, (b) vertical PSD, and (c) along wind-vertical cosprectrum. The black line in (a) and (b) is to indicate the $f^{-2/3}$ slope characteristic of the inertial subrange. The vertical dashed red lines indicate the range of frequencies corresponding to vortex shedding found in Figure 54.

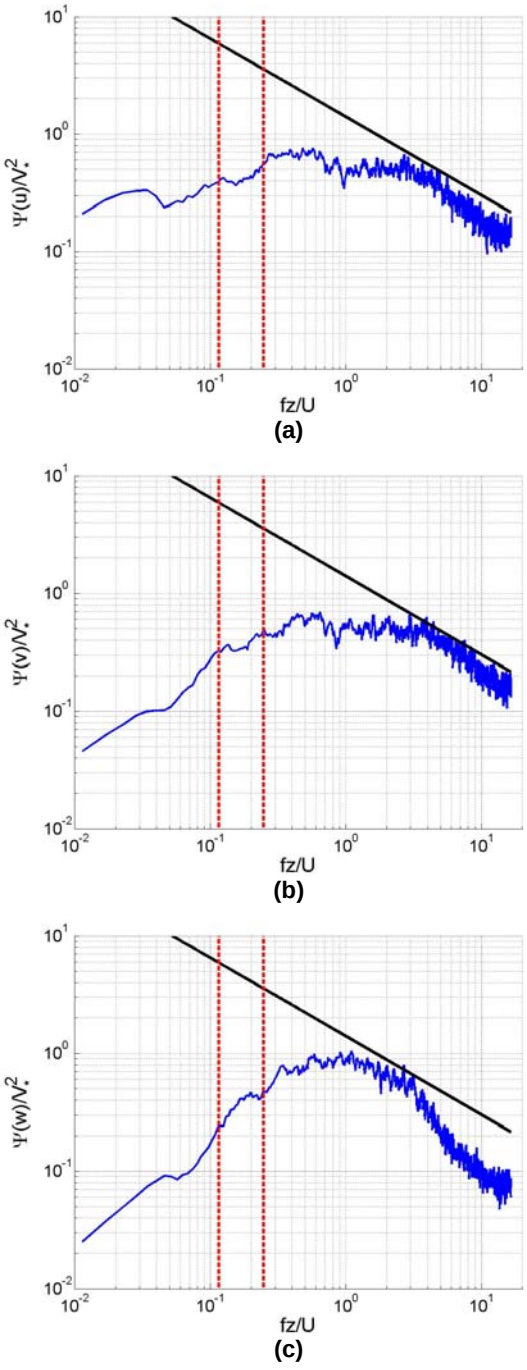

Figure 61. MUST premultiplied spectra obtained from the LANL sonic at z = 2.37 m, located 0.17 m below and 1 m downwind the trailing edge of the container on the south side of the simulated urban canyon. (a) along-wind PSD, (b) cross-wind PSD, and (c) vertical PSD. The black line is to indicate the $f^{-2/3}$ slope characteristic of the inertial subrange. The vertical dashed red lines indicate the range of frequencies corresponding to vortex shedding found in Figure 54.

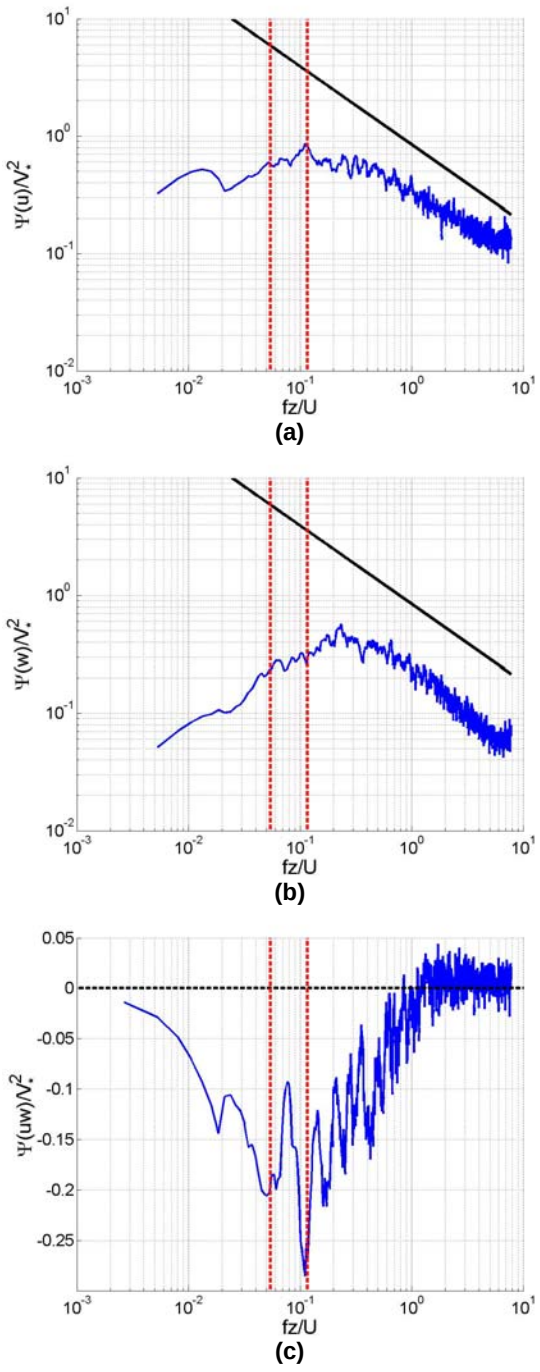

Figure 62. MUST premultiplied spectra obtained from the LANL sonic at z = 1.7 m, located 0.74 m below and 4 m downwind the trailing edge of the container on the south side of the simulated urban canyon. (a) along wind PSD, (b) vertical PSD, and (c) along wind-vertical cosprectrum. The black line in (a) and (b) is to indicate the $f^{-2/3}$ slope characteristic of the inertial subrange. The vertical dashed red lines indicate the range of frequencies corresponding to vortex shedding found in Figure 54.

4. CONCLUSIONS

Turbulence in and around urban areas is the result of a combination of the background turbulence in the ASL surrounding the urban area and sources within the urban area. The amount that each of these effects influence the flow in any one location is dependent on the local morphology of the urban area. Above the buildings the flow is dominated by the ASL conditions, making the flow basically ASL flow that has been modified by the presence of the buildings below it. Deep within the UC the flow tends to be dominated by building effects making the flow basically bluff body flow influenced by the ASL surrounding it. The conditions involved in the transition between these two states are a topic of continuing research and have yet to be clearly defined.

The characteristics of the turbulence vary greatly from one location to another due to localized effects. The complicated geometry of an urban area imposes a variety of flow scales on the turbulence from small-scale phenomena that are typically highly localized to building-scale flow phenomena, which permeate the entire urban canyon. The inherent inhomogeneity of the flow through urban areas requires a measurement density that can be prohibitive. High-density measurements are expensive and difficult to perform in true urban areas, which is why so much effort has been placed into using wind tunnel models to study the flow in urban areas, since high density measurements are relatively easy to perform, upstream conditions are repeatable and the experiments are far less costly. Although these attributes of wind tunnel models are very attractive, these models are unable to capture all of the effects found in true urban areas. Even though both JU03 and MUST were performed in ASL flow, the differences in surface conditions gave very different thermal characteristics between the two experiments. It would be difficult to accurately simulate these effects in a wind tunnel model. The fact that the ratios of ASL depth to building/obstacle height are quite different also presents another difficulty. Artificial ASL are often generated in wind tunnel simulations but it is impossible for these artificial ASL to capture the range of scales present in a true ASL due to simple geometric limitations of wind tunnels. The difference in ASL depth to obstacle height likely increased the influence of the ASL flow aloft on the canyon flow in the MUST array. The differences in geometry also play a major role in the interaction between the ASL flow aloft and the canopy flow, which suggests that models be made as geometrically similar as possible.

The mean turbulence statistics from both JU03 and MUST show a great deal of variability from one location to another. The variability in these statistics makes it difficult to determine scaling parameters characteristic of the urban area. In the absence of a universal similarity theory for urban areas, local scaling parameters were produced using similar methods to those used in the undisturbed ASL. While

a purely local scaling may be appropriate in some cases, quasi-local scaling or inertial sublayer scaling may be more appropriate depending on the amount of interaction between the ASL flow aloft and the canopy flow. The results of Rotach (1993, 1999, and 2001) and Kastner-Klein & Rotach (2004) would support this notion.

The JU03 data exhibited strong channeling throughout the Park Avenue street canyon under oblique upstream flow. The less densely packed obstacles in the MUST array only showed very small channeling effects in center of the simulated street canyon under similar oblique upstream conditions. This demonstrates the difference in the amount of interaction between individual buildings or obstacles on the flow in the canopy for the different area fractions.

The bluff-body flow within urban areas and obstacle arrays locally generate significant mean vertical velocities as opposed to the behavior of ASL flow, which generally exhibits a zero mean vertical velocity. The vertical velocities measured within the Park Avenue canyon may be evidence of a "corkscrew" flow existing within the canyon as suggested by Nakamura and Oke (1988) though there were insufficient measurements to prove this conclusively. The strongest mean vertical velocities measured in MUST were due to the down draft in the wake of an individual obstacle. The strongest mean vertical velocity measured in JU03 was the updraft at the top of a leeward wall in the canyon.

There are a multitude of sources of turbulence in true urban areas: vortex shedding off of buildings, trees, and stationary objects, vehicle traffic, etc. Many of these imposed flow scales are highly localized while others have wide reaching effects. Local effects are evident in both mean statistics and spectra. Mean statistics provide information into the net effect of all flow scales, while the spectra provide more detailed information on how the various flow scales contribute to the mean statistics. Local effects are evident in the mean statistics through deviations from general trends. In spectra imposed flow scales generally act as energy sources injecting energy across discrete frequency bands. The regular array of obstacles in MUST was found to introduce a large amount of energy over a discrete band of frequencies, making the distinction between the upper level flows and those found in the undisturbed ASL more striking. The band of frequencies corresponding to the vortex shedding was also the peak in the PSD. Thus these eddies contain more energy than the larger scale eddies from the ASL turbulence and therefore the vortex shedding appears to dominate the turbulent processes in the canopy and RSL of the array. In true urban areas such as those found in OKC, there is a great variability in the size and shape of the buildings causing the building effects to be more evenly distributed and as such a discrete vortex shedding frequency is not evident throughout the urban area as was found in MUST.

The peak in the along-wind PSD was found to occur at lower frequencies than the peak in the vertical PSD in the data from both JU03 and MUST. In the MUST data where the imposed length scales were uniform throughout the array the peak in the cospectra was generally found to occur at the upper end of the frequencies associated with the vortex shedding off of the obstacles. Local effects at street level in the Park Avenue street canyon often produce positive along-canyon to vertical velocity cospectra over some of the lower frequency bands in the lowest 10% of the canyon. This contradicts typical ASL flow, which exhibits predominantly negative along-canyon to vertical velocity cospectra. This behavior was not found in the MUST cospectra, which was found to have negative over all measured frequencies for all of the sonic anemometers presented in this manuscript.

Proximity of vertical walls was found to have major effects on the mean turbulence statistics and spectra. The effect was most striking in the PSD of the velocity component perpendicular to the wall surface, manifesting as an expanded f^{-1} region. In JU03 this region was found to extend nearly the entire range of frequencies measured.

5. REFERENCES

Biltoft, C., 2001: Customer report for Mock Urban Setting Test. Rep. no. WDTC-FR-01-121, US Army Dugway Proving Ground.

Burian, S. J., Han, W. S., and Brown, M. J., 2003: Morphological analyses using 3D building databases: Oklahoma City, Oklahoma. Los Alamos National Laboratory Report.

Cheng, H. and Castro, I. P., 2002a: Near wall flow over urban-like roughness. *B. Layer. Meteo.*, **104**, 229-259

Cheng, H. and Castro, I. P., 2002b: Near-wall flow development after a step change in surface roughnesses. *B. Layer. Meteo.*, **105**, 411-432

Drobinski, P., Carlotti, P., Newsom, R. K., Banta, R. M., Foster, R. C., and Redelsperger, J.-L., 2004: The structure of the near-neutral atmospheric surface layer. *J. Atmos. Sci.*, **61**, 699-714.

Hanna, S. R., Tehranian, S., Carissimo, B., MacDonald, R. W., and Lohner, R., 2002: Comparisons of model simulations with observations of mean flow and turbulence within simple obstacle arrays. *Atmos. Env.*, **36**, 5067-5079.

Hunt, J. C. R. and Carlotti, P., 2001: Statistical structure at the wall of the high Reynolds number turbulent boundary layer. *Flow Turbul. Combust.*, **66**,453-475.

Kastner-Klein, P. and Rotach, M. W., 2004: Mean flow and turbulence characteristics in an urban roughness sublayer. *B. Layer Meteo.*, **111**,55-84.

Nakamura, Y. and Oke, T., 1988: Wind, temperature, and stability conditions in an east-west oriented canyon. *Atmos. Env.*, **22**, 2691-2700.

Nelson, M. A., Brown, M. J., Klewicki, J. C., and Pardyjak, E. R., 2004a: Variation of flow within the MUST building array. **P2.2**, 5th AMS Urban Env. Symp., Vancouver, B.C., Canada

Nelson, M. A., Brown, M. J., Pardyjak, E. R., and Klewicki, J. C., 2004b: Area-averaged profiles over the Mock Urban Setting Test array. **15.2**, 5th AMS Urban Env. Symp., Vancouver, B.C., Canada.

Oke, T. R., 1987: *Boundary Layer Climates*. London: Routledge, 2nd Ed.

Rotach, M. W., 1993: Turbulence close to a rough urban surface, Part I: Reynolds stress. *B. Layer Meteo.*, **65**, 1-28.

Rotach, M. W., 1999: On the influence of the urban roughness sublayer on turbulence and dispersion. *Atmos. Env.*, **33**, 4001-4008.

Rotach, M. W., 2001: Simulation of urban-scale dispersion using a lagrangian stochastic dispersion model. *B. Layer Meteo.*, **99**, 379-410.

Yee, E., and Biltoft, C. A., 2004: Concentration fluctuation measurements in a plume dispersing through a regular array of obstacles. *B. Layer Meteo.*, **111**,363-415.